Wolframin is a novel regulator of tau pathology and neurodegeneration

Shuo Chen[1,2], Diana Acosta[1,#], Liangping Li[1,#], Jiawen Liang[1], Yuzhou Chang[2,3], Cankun Wang[3], Julie Fitzgerald[1], Cody Morrison[1], Chris N. Goulbourne[4], Yoshi Nakano[5], Nancy C. Hernandez Villegas[5,6], Lalitha Venkataraman[1,7], Cris Brown[8], Geidy E. Serrano[9], Erica Bell[10], Trina Wemlinger[11], Min Wu[1], Olga N. Kokiko-Cochran[1], Phillip Popovich[1], Xena E. Flowers[12], Lawrence S. Honig[12], Jean Paul Vonsattel[12], Douglas W. Scharre[10], Thomas G. Beach[9], Qin Ma[3], Jeff Kuret[13], Sulev Kõks[14], Fumihiko Urano[8], Karen E. Duff[5,15], and Hongjun Fu[1,16,*]

[1]Department of Neuroscience, [2]Biomedical Sciences Graduate Program, [3]Department of Biomedical Informatics, [10]Department of Neurology, Center for Cognitive and Memory Disorders, Center for Neuromodulation, [11]Clinical Research Center, Clinical Trials Management Organization, [13]Department of Biological Chemistry & Pharmacology, and [16]Discovery Theme on Chronic Brain Injury, The Ohio State University, Columbus, OH, USA;
[4]Center for Dementia Research, The Nathan S. Kline Institute for Psychiatric Research, New York, NY, USA; [5]Department of Pathology and Cell Biology, Columbia University Medical Center, New York, NY, USA; [6]Current address: Helen Wills Neuroscience Institute, University of California, Berkeley, Berkeley, CA, USA; [7]Center for Gene Therapy, Nationwide Children's Hospital, Columbus, OH, USA; [8]Department of Medicine, Washington University School of Medicine, St. Louis, MO, USA; [9]Banner Sun Health Research Institute, Sun City, AZ, USA; [12]Department of Neurology, Columbia University Irving Medical Center, New York, NY, USA; [14]Centre for Molecular Medicine and Innovative Therapeutics, Murdoch University, Perth, WA, Australia; Perron Institute for Neurological and Translational Science, Perth, WA, Australia; [15]UK Dementia Research Institute, UCL Queen Square Institute of Neurology, London, United Kingdom;
# Both authors contributed equally.
* Correspondence should be addressed to Hongjun Fu at Hongjun.Fu@osumc.edu.

Abstract

Selective neuronal vulnerability to protein aggregation is found in many neurodegenerative diseases including Alzheimer's disease (AD). Understanding the molecular origins of this selective vulnerability is therefore of fundamental importance. Tau protein aggregates have been found in

Wolframin (WFS1)-expressing excitatory neurons in the entorhinal cortex, one of the earliest affected regions in AD. The role of WFS1 in Tauopathies and its levels in tau pathology-associated neurodegeneration, however, is largely unknown. Here we report WFS1 deficiency is associated with increased tau pathology and neurodegeneration, whereas overexpression of WFS1 reduces those changes. We also find that WFS1 interacts with tau protein and controls the susceptibility to tau pathology. Furthermore, chronic ER stress- and autophagy-lysosome pathway (ALP)-associated genes are enriched in WFS1-high excitatory neurons in human AD at early Braak stages. The protein levels of ER stress- and autophagy-lysosome pathway (ALP)-associated proteins are changed in tau transgenic mice with WFS1 deficiency, while overexpression of WFS1 reverses those changes. This work demonstrates a possible role for WFS1 in the regulation of tau pathology and neurodegeneration via chronic ER stress and the downstream ALP. Our findings provide insights into mechanisms that underpin selective neuronal vulnerability, and for developing new therapeutics to protect vulnerable neurons in AD.

Keywords: Wolframin, WFS1, tau pathology, neuronal vulnerability, Alzheimer's disease, neurodegeneration, ER stress, autophagy-lysosome pathway, entorhinal cortex.

Introduction

Alzheimer's disease (AD) is biologically characterized by amyloid β (Aβ) deposition, pathologic tau, and neurodegeneration (ATN) [29]. Pathologic tau correlates better with neurodegeneration and cognitive deficits than Aβ deposition [30, 31]. Prevailing evidence suggests that Aβ acts primarily as a trigger of various downstream processes, in particular tau aggregation, which induces neurodegeneration [35, 49, 66]. Previous studies from our group and others have shown

that excitatory (EX) neurons in the superficial layer of the entorhinal cortex (EC) are preferentially vulnerable to tau pathology in human AD at early Braak stages with mild/moderate tau pathology and tau transgenic (Tg) mouse models [6, 20, 52, 53, 67]. By utilizing a tau Tg mouse model, we have previously identified that grid cells (a cluster of EX neurons in layers II/III of the EC that form part of the spatial navigation system [54]) are specifically vulnerable to pathologic tau accumulation, resulting in grid cell dysfunction and associated spatial memory deficits [20]. Interestingly, one of the molecular characteristics of grid cells is a strong expression of wolframin (WFS1) [37, 38]. Indeed, one recent study has identified that pathological tau is accumulated in WFS1-positive (+) EX neurons in early AD cases with mild/moderate tau pathology, and the number of double-positive neurons with both pathological tau and WFS1 is reduced in late AD cases with severe tau pathology [12]. Although this evidence suggests that $WFS1^{+}$ cells may be vulnerable to tau pathology in AD, the underlying mechanisms that contribute to the selective vulnerability of WFS1-expressing EX neurons to tau pathology and neurodegeneration are still not completely understood.

WFS1, a transmembrane glycoprotein localized to the endoplasmic reticulum (ER) [68], has been shown to be a component of the unfolded protein response (UPR) that mitigates ER stress response to unfolded or misfolded proteins in cells [14, 15]. Pathogenic variants in the *WFS1* gene cause Wolfram syndrome, an autosomal recessive disorder characterized by juvenile-onset diabetes, optic atrophy, and progressive neurodegeneration [43, 70]. Neuronal knockdown of *wfs1* has been found to increase the susceptibility to axon degeneration caused by overexpression of human tau in *Drosophila* [61]. Forced overexpression of human *P301L* mutant tau in WFS1-expressing neurons of mouse medial EC-II using a Flex-AAV viral vector system can spread tau to the hippocampal CA1 region in *Wfs1-Cre* mice [12], suggesting WFS1 may also be involved in

the propagation of tau pathology. The role of WFS1 in AD-associated tau pathology and neurodegeneration is, however, largely unknown.

Accumulating evidence indicates that β cell death and neuronal cell dysfunction in Wolfram syndrome are attributed to high levels of ER stress signaling in affected cells [14, 34, 60, 73]. WFS1 deficiency induces chronic ER stress, cytosolic Ca^{2+} dyshomeostasis, and mitochondrial abnormalities [7], which are also found in neurodegenerative diseases including AD [1, 25, 43, 49, 57]. Although the physiological level of ER stress can enhance the ER-associated degradation (ERAD) of unfolded or misfolded proteins via the autophagy-lysosome pathway (ALP) [21, 58], chronic ER stress has been found to block autophagy flux and inhibit the degradation and clearance of misfolded proteins [55, 58]. Likewise evidence indicates ER stress and ALP are interlinked and implicated in the degradation and clearance of pathologic tau [4, 24, 64]. We hypothesized that reducing WFS1 induces chronic ER stress and blocks the downstream ALP, resulting in the acceleration of tau pathology and neurodegeneration; whereas enhancing WFS1 protects excitatory neurons against tau pathology and neurodegeneration via the inhibition of chronic ER stress and the upregulation of ALP. Here we compared the protein levels of WFS1 and the number of WFS1-expressing cells in human AD and tau mice with aged-matched controls. We also investigated the effects of loss-of-function and gain-of-function of WFS1 on tau pathology, astrogliosis, postsynaptic degeneration, apoptosis and cognitive deficits in PS19 tau mice [76]. Then we explored the mechanisms underlying the selective vulnerability of WFS1-expressing EX neurons to tau pathology by measuring the subcellular localization of WFS1 and tau proteins as well as their interaction, determining the effect of WFS1 overexpression on tau seeding, analyzing our 10x Visium spatial transcriptomic datasets from human postmortem AD and control brains

and publicly available single-nucleus RNA-Seq datasets, and measuring the protein levels of key players of chronic ER stress and ALP in PS19 tau mice with deficiency or overexpression of WFS1.

Methods

Animals

EC-tau mice [45] were generated by crossing the neuropsin-tTA activator line with a tetracycline-inducible tau P301L responder line. PS19 tau mice (Stock No: 008169) and control B6C3 mice (Stock No: 100010) were purchased from the Jackson Laboratory. The *Wfs1* knockout (*Wfs1*$^{-/-}$) mice [39] were provided by the University of Tartu, Estonia. The control 129S6 mice were purchased from Taconic. The F1 offspring (both males and females) were used as experimental animals. All animals were maintained on a 12-hour light/dark cycle with food and water provided ad libitum. All animal experiments were performed in accordance with national guidelines (National Institutes of Health) and approved by the Institutional Animal Care and Use Committee of The Ohio State University and Columbia University. Mice were anesthetized and perfused transcardially by 0.05% heparin in 1x phosphate-buffered saline (PBS). Harvested brains were separated into two hemispheres. The left hemisphere was fresh frozen immediately on dry ice and stored at -80°C for total protein extraction, while the right hemisphere was immersed and fixed in the 10% formalin overnight at 4°C for immunofluorescence (IF) staining.

Human postmortem brain tissues.

Human fresh frozen brain blocks were provided by the Arizona Study of Aging and Neurodegenerative Disorders/Brain and Body Donation Program at Banner Sun Health Research Institute [3], the New York Brain Bank at Columbia University Irving Medical Center [71], and the Brain Bank & Biorepository at Ohio State University Wexner Medical Center. The

demographics and neuropathology of human cases used in this study are listed in **Table 1**. This research involves specimens from deceased persons, with sample de-identification, and as such the IRB has determined this not human subject research. Frozen sections (10 μm) were cut from frozen blocks under RNase-free conditions.

Reagents

Human conformation-dependent tau, MC1, is a monoclonal antibody raised to paired helical filaments and recognizes conformational epitopes on recombinant tau [32]. The reactivity of MC1 depends on both the N terminus (amino acids 7–9), and an amino acid sequence of tau (amino acids 313–322) in the third microtubule binding domain. In addition to MC1, total Tau (DA9), and human/murine phospho-tau pSer396/ Ser404 (PHF1) monoclonal antibodies were provided by Peter Davies. Human/murine phospho-tau pSer202/Thr205 (AT8, Cat# MN1020), Tau46 (Cat# 13-6400), and Alexa Fluor dye-labeled cross-absorbed donkey secondary antibodies were purchased from ThermoFisher Scientific. Sheep anti-WFS1 (Cat# AF7417) was purchased from R&D systems. Mouse anti-PSD95 (Cat# 810302) antibody and chicken anti-GFAP (Cat# 829401) was purchased from BioLegend. Rabbit anti-GFAP (Cat# G9269), TauC (Cat # A0024), p62 (Cat# NBP1-48320SS) polyclonal antibodies, and Sudan Black B (Cat# 199664) were purchased from Sigma-Aldrich, DAKO, and Novus Biologicals, respectively. Rabbit anti-WFS1 (Cat# 1158-1-AP), CHOP (Cat# 15204-1-AP), CTSD (Cat# 21327-1-AP), and TFEB (Cat# 13372-1-AP) antibodies were purchased from Proteintech. Rabbit anti-ATF4 antibody (Cat# 11815) was purchased from Cell Signaling Technology. Rabbit anti-SATB2 (Cat# ab92446) and pS396 tau (Cat# ab109390) antibodies were purchased from Abcam. Hoechst33342 (Cat# 14533) were purchased from Sigma-Aldrich. TrueBlack lipofuscin autofluorescence quencher (Cat# 23007) was purchased from Biotium. Fluoromount-G Mounting Medium (Cat# 0100-01) was purchased

from SouthernBiotech. The pLenti-hWFS1 and control lentiviruses, AAV9-CMV-hWFS1-IRES-GFP, and control AAV9-CMV-IRES-GFP viruses were generated by the Hope Center Viral Vectors Core at Washington University in St. Louis. The RD-P301S-YFP lentivirus and DS9 tau cell line [62] were provided by Marc Diamond.

IF staining

IF staining was performed as previously described [20]. Free-floating sections from mouse brains were incubated with 10 mM sodium citrate antigen retrieval buffer (pH6.0) at 95°C for 12 min. After antigen retrieval, the sections were washed by 1x PBS and blocked with 10% donkey serum in 0.3% PBS Triton X-100 (PBST) for 1 hour at room temperature. Primary antibody incubations were performed overnight at 4°C. On the second day, sections were washed three times by 0.1% PBST and then incubated with secondary antibodies (1:1000) at room temperature for 2 hours. After three washes with 1x PBS, sections were mounted, and autofluorescence was quenched with 0.3% Sudan Black B in 70% ethanol for 5 min. The nuclei were stained with 5 μg/mL Hoechst33342 in 0.3% PBST for 9 min at room temperature. Sections were sealed with Fluoromount-G Mounting Medium and were imaged with a Zeiss Axio Observer microscope.

For human FFPE brain samples, the sections were first deparaffinized and rehydrated before performing antigen retrieval as described above. For the human fresh frozen sections, slides were air dried at 37°C for 10 min and then fixed and permeabilized by prechilled acetone at -20 °C for 15 min before antigen retrieval. Following antigen retrieval, slides were washes three times with 1x PBS and were then immersed into 0.3% PBST 15 min for permeabilization before blocking for 1-hour with 10% donkey serum in 0.3% PBST. Primary antibodies were incubated overnight at 4°C. Secondary antibodies were diluted 1:1000 in the blocking buffer and incubated with sections at room temperature for 3 hours. The nuclei were stained with Hoechst33342 in the same way as

mouse brain sections. Autofluorescence was quenched with 0.5x TrueBlack solution in 70% ethanol for 10 min, followed by three washes with 1x PBS. The coverslips were mounted with Fluoromount-G Mounting Medium, and the slides were then imaged with a Leica confocal microscope with a 63x objective.

Electron microscopy

Ultrastructural analyses were performed in mouse brain sections following immunogold labeling. Post-embedding immunogold labeling was performed as described [44, 75]. Mice were anesthetized with a mixture of ketamine (100 mg/kg) and xylazine (10 mg/kg) and perfused transcardially by 0.05% heparin in 1x PBS followed by 50 ml ice-cold fixative (2.5% glutaldehyde, 2% paraformaldhyde in 0.1 M sodium cacodylate buffer, pH 7.4; Electron Microscopy Sciences Catalog#15960-01). Mouse brains were harvested and immersed in the same fixative overnight at 4°C. Mouse hemi brains were embedded in 2% agarose gel and cut into 80-μm vibratome sections, which were then dehydrated in a graded series of ethanol and embedded in Spurr Resin (Electron Microscopy Sciences). The processed vibratome sections were further cut into 60-nm ultrathin sections. Ultrathin sections were mounted on grids and etched for 5 min with 1% sodium metaperiodate in 1x PBS. Ultrathin sections were then incubated sequentially in blocking solution (5% horse serum in 1x PBS containing 0.2% Tween 20), primary antibodies (MC1, WFS1, and DA9, 1:1 dilution, overnight at 4°C) and secondary antibodies conjugated with 6 nm or 10 nm gold (room temperature, 2 hours). The sections were observed with a transmission electron microscope (ThermoFisher Talos L120C).

Duolink proximity ligation assay (PLA)

Duolink probes and detection reagents (red) kits were purchased from Sigma-Aldrich (Duo92002, Duo92004, and Duo92008). Fixation, antigen retrieval, and blocking were performed in the same

way as the IF staining of mouse and human brain sections described above. WFS1 and Tau antibodies (AT8 or Tau46) were incubated sequentially to avoid artificial co-localization of two antibodies. Briefly, fresh frozen sections were incubated with WFS1 primary antibody (1:2000) in a humidity chamber for 3 hours at 37°C. Following three washes by 0.1% PBST, brain sections were incubated with Tau antibodies (1:500) overnight at 4°C. Slides were washed three times in 0.1% PBST, and then incubated with PLA probes mixture (1:6 dilution mixture of anti-mouse plus and anti-rabbit minus probes) in the humidity chamber at 37°C for 1 hour. The amplification reaction was extended to 200 min after 1 hour ligation on mouse and human brain sections. The sections were then incubated with Hoechst33342 to stain the nuclei. Autofluorescence was quenched with 0.5x TrueBlack solution in 70% ethanol for 10 min and was washed off by 1x PBS. The coverslips were mounted with Fluoromount-G Mounting Medium, and the slides were then imaged with a Leica confocal microscope with a 63x objective. The number of Duolink red dots representing the interactions were counted and quantified by Fiji, and the data was analyzed by Prism 5 software.

Tau seeding assay

The stable cell line SH-SY5Y harboring RD *P301S* mutant tau was generated using the RD-P301S-YFP lentivirus provided by Marc Diamond, and the cell colony was selected using the cloning cylinder. The stable tau cell line was then transfected with different concentrations of control and hWFS1 lentivirus (1:1000, 1:500, 1:250). Representative live images of tau aggregates were taken 24 hours after incubation with 2 μg DS9 tau seeds, which were isolated from DS9 cell lines as previously described [62]. Transduction of tau seeds was aided by incubating samples with lipofectamine-3000 (Invitrogen) at room temp for 20 minutes prior to seeding. Then cells were fixed with 4% PFA and the immunostaining of WFS1 was performed to validate its overexpression.

Extraction of total protein, Sarkosyl-soluble, and Sarkosyl-insoluble fractions

Fresh frozen mouse brains were homogenized in 1x RIPA buffer containing the Protease & Phosphatase inhibitor Cocktail (P&P inhibitor, Thermo Scientific, Cat# 78441) and 1 mM phenylmethyl-sulfonyl (PMSF) using 1.4-mm ceramic beads (Cat# 19-627-3). Homogenates were centrifuged at 5,000 g for 20 min at 4 °C. The supernatant was saved as total protein. The concentration of total protein was measured and quantified by BCA assay. Five hundred microgram of the total protein extracts were normalized into 500 µl of 1% Sarkosyl RIPA buffer with 1x P&P inhibitor and 1mM PMSF. Aliquots were incubated on a rotor at 4°C overnight and then spun at 100,000 g for 1 hour at 4°C. The supernatant was transferred to a new tube as Sarkosyl-soluble protein, while the pellet was resuspended in 50 µl Tris-urea buffer (50 mM pH7.5 Tris-HCl buffer with 8 M urea containing the P&P inhibitor and 1 mM PMSF) as Sarkosyl-insoluble protein. Total protein, Sarkosyl-soluble, and Sarkosy-insoluble fractions were saved at -80°C for Western Blot assay or Meso Scale Discovery (MSD) multi-spot phospho(Thr231)/total tau assay.

Western blot assay

Total protein, Sarkosyl-soluble, and Sarkosy-insoluble fractions were electrophoretically separated by running 10 µg protein lysates on 4-12% Bis-Tris precast polyacrylamide gels and blotted using nitrocellulose blotting membranes. Target proteins were probed with primary antibodies overnight at 4°C on a shaker. The membranes were incubated with Li-Cor fluorescent secondary antibodies for 1 hour at room temperature. The membranes were then imaged using a Li-Cor Imager.

MSD multi-spot phospho(Thr231)/total tau assay

The 96-well phospho(Thr231)/total tau plates were obtained from MSD (Cat# K15121D-1), and multi-spot immunoassay was performed following manufacturer's protocol. The plate was first blocked for 1 hour at room temperature with 3% Blocker A solution in 1x Tris wash buffer, then washed four times with 1x Tris wash buffer. 25 µl of Tau441 calibrator or samples were added to the corresponding wells and incubated on a shaker at room temperature for 1 hour. After four washes with 1x Tris wash buffer, 25 µl of SULFO-TAG detection antibody solution was added to each well and incubated on a shaker at room temperature for 1 hour. The antibody solution was then washed off by 1x Tris wash buffer, and 150 µl/well of Read Buffer T was added. The plate was read with a MESO QuickPlex SQ 120 instrument.

Terminal deoxynucleotidyl transferase-mediated dUTP-biotin nick end labeling (TUNEL) assay

TUNEL assay was performed using the In Situ Cell Death Detection Kit-TMR red from Roche (Cat# 12156792910). The protocol was modified to optimize the staining on free-floating mouse brain sections. The section was incubated in 10 mM sodium citrate (pH6.0) at 95°C for 12 min for antigen retrieval. After three washes with 1x PBS, the section was incubated in 0.3% PBST at 37°C for 20 min for permeabilization. Premixed TUNEL reaction mixture (Enzyme solution/label solution = 1:9) was prepared in a 200 µl tube. Permeabilized sections were incubated with the TUNEL reaction mixture at 37°C for 2 hours in the dark. The sections were than washed twice with 1x PBS, and the nuclei were stained by Hoechst33342.

Stereotaxic surgery

Stereotaxic viral injections were performed in accordance with IACUC guidelines of The Ohio State University. Mice were anesthetized by placing them in a closed plastic box connected to an Isoflurane system (Patterson veterinary, CO, USA) prior to surgery. Mice were then placed on a

stereotaxic instrument (RWD Life Science, China) and were maintained anesthetized via a nose cone, which allowed for constant flow of isoflurane (1.5–2% by volume) throughout the surgery. Viruses were injected by using a 10-μl Hamilton microsyringe (GASTIGHT #1701) attached with a 30-gauge needle. A microsyringe pump (KD Scientific, MA, USA) was used to control the speed of injection at 100 nl/min. The delivery of AAV9-CMV-hWFS1-IRES-GFP or control AAV9-CMV-IRES-GFP viruses was directed into the MEC (500 nl) using the following coordinates, AP, −4.7 mm; ML, ±3.3 mm; and DV, −3.3 mm and ventral hippocampus (750 nl) using coordinates, AP, −3.4 mm; ML, +3.1 mm; and DV, −3.3 mm, according to the mouse brain atlas of Paxinos and Franklin's (fourth edition). After injection, the needle remained in the target site for 10 minutes.

Behavioral tests

A Y-maze constructed of three identical arms of opaque plastic (40 × 4.5 × 12 cm) 120° apart was placed in the center of a room with a dim light of 30 lux brightness. Visual cues were located in the periphery of the room (or on the wall of each arm) to allow visual orientation. Each mouse was placed at the end of one arm facing the center and allowed to freely explore the apparatus. Experiments were video recorded through a camera mounted above the apparatus. Animal behavior was scored by using the automatic video tracking system (ANY-maze). Entries into each arm were scored for 10 minutes. Alternation behavior was determined from successive entries of the three arms without repetition (for example, ABC, BCA, CAB...). The percentage of spontaneous alternation was calculated as the actual alternations divided by the possible alternation (total arm entries − 2) × 100. The mice with total entries ≤ 2 were excluded from the analysis.

A Barnes-maze with a 91-cm-diameter circular arena contained 18 evenly distributed holes on the perimeter with one target hole (leading animals to a dark escape box). During the 5-day training session, mice were first placed onto the center of the maze individually. Experiments were video

recorded for 120 sec/trial and 3 trials/day. On the 6th day, the escape box was removed, and a probe test was performed for each mouse. The mouse was placed on the maze for 90sec, and their time spent in the Q3 quadrant containing the target hole was recorded and assessed using ANY-maze. It should be noted that mice do not always enter the goal box during the probe test of Barnes maze, which can skew escape latency data. To identify mice that sit near the escape hole without entering, we evaluated the time (latency) to find the goal perimeter, which was operationally defined at the 1.5-inch perimeter around the goal hole on top of the Barnes maze. Analyzing the latency to goal perimeter provided a way to identify the time that experimental mice took to traverse to the goal, but do not actually enter the goal box.

Spatial transcriptomics (ST) experiment and GO enrichment analysis

The sample selection and preparation for ST, ST processing, and IF on adjacent sections were performed as we recently described [8]. Briefly, the 10x Genomics Visium Spatial Transcriptome experiment was performed according to the User Guide of 10x Genomics Visium Spatial Gene Expression Reagent Kits (CG00239 Rev D), and fresh frozen postmortem human brain was sectioned into 10 μm and mounted on the 10x Gene Expression slide (Part# 1000188). One adjacent section was saved for WFS1/AT8 co-staining, and the staining was then aligned to the H&E image on the Gene Expression slide using the "Transform/Landmark correspondences" plugin in Fiji. The spots with WFS1 and AT8 staining in aligned image were marked as WFS1$^+$/AT8$^+$ spots, and the gene expression levels in those spots were compared with the adjacent spots using Seurat function *FindMarkers*. Differentially expressed genes (DEGs) from WFS1$^+$/AT8$^+$ spots were then subjected to GO enrichment analysis using the *enrichGO* function in R package clusterProfiler (v.3.18.0) [77]. Visium data and staining images could be found and downloaded from our in-house website (https://bmbls.bmi.osumc.edu/scread/stofad).

For the single-nucleus RNA-seq analysis, we used human EC datasets [42] GSE147528 downloaded from Gene Expression Omnibus. DEGs were assessed with the Seurat function *FindMarkers* by comparing EX neurons from human EC at Braak stage 0 (control), 2, and 6. Gene set enrichment analysis was performed using the Enrichr web server [40].

Statistical analysis

No statistical methods were used to predetermine sample sizes. Prism 5 software was used to analyze the data. All data are expressed as mean ± SEM. We performed the D'Agostino–Pearson omnibus normality test to determine whether the data were normally distributed. Then we chose the Nonparametric Mann-Whitney tests were used to compare the numbers of marker-positive cells (MC1, WFS1, SATB2, TUNEL, and p62), Duolink dots, the mean intensity of the IF staining (GFAP, PSD95, ATF4, CHOP, CTSD, and TFEB), or percentage of area of the tau seeds signal from each paired group. All results represent two-sided tests comparing groups of biological replicates. $P < 0.05$ was considered statistically significant for all measures. The *n* values represent the number of mice, cases, spots or cells in each group; exact values are indicated in figure legends.

Results

WFS1-expressing EX neurons in layers II/III of the EC are vulnerable in tau mouse models, human AD and other types of proteinopathies.

Previous findings indicate that grid cells in the EC are crucial components of the spatial navigation system [54], are vulnerable in a tau mouse model (EC-tau) [20], and certain grid cells express WFS1 [38]. One recent study has identified that WFS1-positive (+) EX neurons are vulnerable to pathological tau, and WFS1 is reduced in AD cases with severe tau pathology [12]. Whether WFS1 is altered in AD with mild/moderate tau pathology and in other types of proteinopathies, however,

has not been fully investigated. Therefore, we set out to test if WFS1 is altered in tau mice and human AD and several other types of proteinopathies, including frontotemporal lobar degeneration with tau pathology (FTLD-Tau) (a non-AD tauopathy), frontotemporal lobar degeneration with transactive response DNA-binding protein (FTLD-TDP), and diffuse lewy body disease (DLBD) (both non-tauopathy proteinopathies). EC-tau mice overexpress human *P301L* mutant tau [11, 45] and exhibit a similar spatial and temporal distribution of tau pathology in comparison to human AD [6]. Using sequential immunofluorescence (IF) staining, we found that pathological tau ($MC1^+$) was partially accumulated in $WFS1^+$ EX neurons ($SATB2^+$) in layers II/III of EC in human AD, EC-tau mice, and PS19 tau mice [76] (**Figs. 1a** and **1b; Supplementary Fig.1a**), and the number of $WFS1^+$ neurons in the EC was significantly reduced in human AD and EC-tau mice compared to controls (**Figs. 1c-f**). A significant reduction of WFS1+ neurons was also found in human FTLD-Tau, FTLD-TDP and DLBD compared to control (CT) cases (**Supplementary Fig. 2**). Furthermore, the protein level of WFS1 measured by Western blot assay was significantly reduced in the EC of human AD cases (Braak stages III-IV) with moderate tau pathology compared to controls (**Figs. 1g** and **1i**). These results suggest that WFS1-expressing EX neurons in the EC are vulnerable in AD and accumulate tau pathology, which is consistent with its main distribution in layers II/III of the EC [36, 38] and may subsequently contribute to the preferential vulnerability of this region in early Braak stages of AD [17]. We further probed the protein expression of WFS1 in FTLD-Tau, FTLD-TDP and DLBD. Interestingly, we observe significant reductions in the protein level of WFS1 in all neurodegenerative cases (FTLD-Tau, FTLD-TDP, and DLBD compared to controls) (**Figs. 1h** and **1j**). These data suggest that abnormal WFS1 expression may also play a role in the pathogenesis of other types of proteinopathies besides AD. The role of WFS1

expression in the pathogenesis of these other types of proteinopathies is beyond the scope of this current work.

WFS1 deficiency is associated with increased tau pathology, astrogliosis, postsynaptic degeneration, apoptosis and cognitive deficits in PS19 tau mice.

Our evidence suggests that EX neurons of the EC that express WFS1 accumulate pathological tau, however, whether the presence or absence of WFS1 may alter pathological tau levels and associated neurodegeneration is unknown. Therefore, in order to investigate the consequences of decreased WFS1 levels on tau pathology and neurodegeneration, we crossed whole-body *Wfs1* knockout (*Wfs1*$^{-/-}$) mice [39] with a widely used tau animal model, PS19 tau mice, which exhibit spatiotemporal distribution of tau pathology, gliosis, neuronal loss and cognitive deficits after 9 months of age [76]. We measured the protein levels of WFS1, total tau (TauC) and phosphorylated tau (PHF1, pS396/S404 tau) in the total protein, sarkosyl-soluble (SS) and sarkosyl-insoluble (SI) lysates from the cortex of 8.7-mo-old mice. Parental PS19 mice at this age show mild tau pathology [76]. First, we validated that the WFS1 protein was reduced by ~50% and 100% in PS19;*Wfs1*$^{+/-}$ and PS19;*Wfs1*$^{-/-}$ mice, respectively, compared to PS19 mice (**Figs. 2a** and **2b**). The reduction in WFS1 was associated with increased pathological tau as indicated by significantly increased ratios of PHF1/TauC in SS and SI lysates of both PS19;*Wfs1*$^{+/-}$ and PS19;*Wfs1*$^{-/-}$ mice (**Figs. 2a**, **2c** and **2d**). Furthermore, the total tau and pT231 tau was measured using the MSD Phospho(Thr231)/Total Tau ELISA kit. The ratio of pT231 tau/total tau in the SI lysates was significantly increased in both PS19;*Wfs1*$^{+/-}$ and PS19;*Wfs1*$^{-/-}$ mice compared to PS19 mice (**Fig. 2h**), and a positive trend indicated increases in the ratio of pT231 tau/total tau in the SS lysates of PS19;*Wfs1*$^{-/-}$ mice compared to PS19 mice (**Fig. 2f**). In both SS and SI lysates, however, the ratio

of pT231 tau/total tau was not significantly changed in *Wfs1*$^{+/-}$ and *Wfs1*$^{-/-}$ mice compared to wild-type (WT) controls (**Figs. 2e** and **2g**). The immunostaining results also showed a significant increase of MC1^{+} cells in the EC of both PS19;*Wfs1*$^{+/-}$ and PS19;*Wfs1*$^{-/-}$ mice compared to PS19 mice (**Figs. 3a** and **3b**). Similarly, tau pathology in cells evidenced by other pTau antibodies (AT8, and PHF1) was also increased in PS19;*Wfs1*$^{+/-}$ mice compared to PS19 mice (**Supplementary Fig.3**). Importantly, pathological tau that was MC1^{+} or pTau^{+} were also found in the deep layer of the neocortex beside the DG and CA1 of the hippocampus and the superficial layer of the cortex in both PS19;*Wfs1*$^{+/-}$ and PS19;*Wfs1*$^{-/-}$ mice (**Fig. 3a**; **Supplementary Fig.3**); however, these pathological tau regions have not been observed in age- and gender-matched PS19 mice, suggesting that WFS1 deficiency is associated with increased tau pathology in PS19 mice which typically exhibit mild tau pathology. These results indicate WFS1 deficiency may promote the propagation and aggregation of pathological tau, which is considered to play important roles in the neuronal and regional vulnerability of AD [26, 33, 56].

Tau pathology has been found to induce astrogliosis, synaptic dysfunction and neurodegeneration [41, 76]. We also found that increased tau pathology in both PS19;*Wfs1*$^{+/-}$ and PS19;*Wfs1*$^{-/-}$ mice compared to PS19 mice (**Fig. 3a**) was associated with significant increases in GFAP immunoreactivity and hypertrophy (**Figs. 3e** and **3f**), significant decreases in the number of SATB2^{+} EX neurons (**Figs. 3c** and **3d**) and PSD95 (postsynaptic marker) immunoreactivity (**Figs. 3g** and **3h**), and significant increases in the number of apoptotic cells evidenced by TUNEL assay (**Figs. 3i** and **3j**). The *Wfs1*$^{+/-}$ and *Wfs1*$^{-/-}$ mice, however, did not show obvious changes in GFAP and PSD95 immunoreactivity or the number of SATB2^{+} EX neurons and TUNEL^{+} cells compared to WT controls (**Supplementary Fig. 4**). These data indicate that WFS1 deficiency increases the

tau pathology in PS19 mice, which is accompanied by astrogliosis, postsynaptic degeneration, and apoptosis.

To further investigate if WFS1 deficiency affects learning and memory, we performed a battery of neurobehavioral tests including Y-maze and Barnes maze. The percentage of spontaneous alternations in Y-maze testing was significantly reduced in PS19;*Wfs1*$^{+/-}$ mice compared to PS19 mice, and further reduced in PS19;*Wfs1*$^{-/-}$ mice (**Fig. 3k**). The latency to goal perimeter of escape hole during training sessions of Barnes maze testing was significantly increased in PS19;*Wfs1*$^{-/-}$ mice compared to PS19 mice (Days 3-5, **Fig. 3l**), while the time spent in Quadrant 3 (Q3) with escape hole was significantly decreased in PS19;*Wfs1*$^{-/-}$ mice compared to PS19 or PS19;*Wfs1*$^{+/-}$ mice (**Fig. 3m**). The *Wfs1*$^{+/-}$ and *Wfs1*$^{-/-}$ mice, however, did not show significant changes in learning and memory compared to WT controls (**Figs. 3k-m**). These results demonstrate that *Wfs1* deficiency impairs the spatial learning and memory in PS19 mice, but not in WT controls.

Overexpression of WFS1 is associated with attenuated tau pathology, astrogliosis and postsynaptic degeneration in PS19 tau mice.

Following the loss-of-function study of *Wfs1*, we performed a gain-of-function study using the stereotaxic microinjection of AAV9-CMV-hWFS1-IRES-GFP or control AAV9 into the EC and hippocampus of 8-mo-old PS19 mice. Three months following the microinjection, we confirmed WFS1 overexpression in the EC and hippocampus region **(Fig. 4a)** and found significant reductions in the number of MC1^{+} neurons and mean intensity of GFAP immunoreactivity **(Figs. 4a-**and **4b)**, significant increases in the mean intensity of PSD95 immunoreactivity (**Figs. 4c** and **4d)**, and significant decreases in TUNEL^{+} cells **(Figs. 4e** and **4f)**in the EC of hWFS1-injected PS19 mice compared to control AAV9-injected PS19 mice. Our results suggest a strong protection

of WFS1 against tau pathology, astrogliosis, postsynaptic degeneration, and apoptosis in PS19 mice.

WFS1 interacts with tau protein and reduces tau seeding.

Our previous results (**Figs. 2**, **3a**, and **3b**) indicate a critical role of WFS1 in regulating tau protein aggregation. In addition, $MC1^+$ and other $pTau^+$ pathological tau was found in the deep layer of the cortex in both PS19;*Wfs1*$^{+/-}$ and PS19;*Wfs1*$^{-/-}$ mice, but not PS19 mice (**Fig. 3a**; **Supplementary Fig. 3**), suggesting that WFS1 may also play an important role in the propagation of aggregated tau protein. We hypothesized that WFS1 can interact with tau protein and control its aggregation and propagation. To test this hypothesis, we first determined the subcellular localization of these two proteins using co-immuno-electron microscopy. The ER transmembrane glycoprotein WFS1 [68] was found to be colocalized with both human pathological tau stained by MC1 (**Fig. 5a**) and total tau protein stained by DA9 (**Supplementary Fig. 5b**) in the ER and synapses of 9.5-month-old PS19 mice. The specificity of WFS1 antibody was validated by the absence of WFS1 immunoreactivity detected in the negative control, *Wfs1*$^{-/-}$ mice (**Supplementary Fig. 5a**). Using the Duolink proximity ligation assay (PLA), a novel and sensitive method of detecting the protein-protein interaction in situ at endogenous levels [16], we further found that WFS1 interacted with both $AT8^+$ pathological tau (**Figs. 5b-e**) and $Tau46^+$ total tau (**Supplementary Figs. 5c-f**) in EC-tau mice and human AD; whereas there was no protein interaction detected in the negative control, *Wfs1*$^{-/-}$ mice (**Figs. 5b** and **5c**). In addition, overexpression of human WFS1 reduced DS9 tau seeding [62] in SH-SY5Y cells stably expressing human *P301S* mutant tau (**Figs. 5f** and **5h**), and tau aggregates were mostly found in cells without

the overexpression of WFS1 (**Fig. 5g**). These results suggest that WFS1 interacts with tau protein and control its aggregation and propagation.

ER stress and ALP are enriched signaling pathways in WFS1-high EX neurons at early stages of AD.

Next, we explored the molecular mechanisms underlying the vulnerability of WFS1-expressing EX neurons in AD. By analyzing the snRNA-Seq data (GSE147528) [42] from human EC at Braak stage 0 (control), 2 (AD with mild tau pathology), and 6 (AD with severe tau pathology), we found the expression level of *WFS1* mRNA was significantly reduced in EX neurons in human AD cases with Braak stage 6 compared to controls with Braak stage 0 and AD cases with Braak stage 2 (**Fig. 6a**). Further gene ontology (GO) enrichment analysis of differentially expressed genes between WFS1-high (> 2x mean) and WFS1-low (< 2x mean) EX neurons from Braak stage 2 datasets revealed Top 5 signaling pathways enriched in WFS1-high EX neurons of AD cases with mild tau pathology (Braak stage 2), including autophagy, suggesting alterations in autophagy related pathways precede the observed reduction of WFS1 in EX neurons in AD cases with severe tau pathology (Braak stage 6) (**Fig. 6b**). We also used the 10x Genomics Visium spatial transcriptomic platform in combination with co-immunofluorescence staining of WFS1 and AT8 (pS202/T305 tau) to define the gene expression in cortical layer 2 of the human middle temporal gyrus (MTG), a vulnerable region, of AD (Braak stage III-IV). Our data showed that WFS1 was enriched in Layer 2 of the MTG (**Fig. 6c**). Interestingly, endoplasmic reticulum (ER) unfolded protein response (UPR), and autophagy-associated pathways are enriched in $WFS1^{+}/AT8^{+}$ spots, compared to adjacent spots without WFS1 or AT8 in Layer 2 of AD brain samples with mild tau pathology (Braak stage III-IV) (**Fig. 6d**), indicating a protective function of WFS1 in the presence

of tau aggregates may be to degrade tau aggregates via upregulation of ER UPR and the autophagy in WFS1^{+} neurons.

WFS1 deficiency alters key proteins associated with chronic ER stress and ALP in PS19 mice, while WFS1 overexpression reverses these changes.

In line with our results indicating WFS1 may exhibit protective functions against tau pathology and neurodegeneration, previous studies suggest WFS1 deficiency may be detrimental by inducing chronic ER stress, cytosolic Ca^{2+} dyshomeostasis, and mitochondrial abnormalities [7], which are also found in neurodegenerative diseases including AD [1, 25, 43, 57]. Chronic ER stress can further block the autophagy flux and inhibit the degradation and clearance of misfolded proteins [55, 58]. Therefore, we hypothesized that WFS1 deficiency induces chronic ER UPR which results in the impairment of ALP, thereby further increasing pathological tau, astrogliosis, neurodegeneration, and memory deficits.

In order to test this hypothesis, we measured the changes of chronic ER stress markers (e.g. activating transcription factor 4 (ATF4) and C/EBP homologous protein (CHOP)) and ALP-associated proteins such as p62, cathepsin D (CTSD), and transcription factor EB (TFEB) in human AD and PS19 mice with the deficiency or overexpression of WFS1. We found that the immunoreactivity of ATF4 and CHOP and the number of cells with aggregated p62 puncta significantly increased (**Figs. 7a-f**), whereas the immunoreactivity of CTSD and TFEB significantly decreased (**Figs. 7g-j**) in PS19;*Wfs1*$^{+/-}$ and PS19;*Wfs1*$^{-/-}$ compared to PS19 mice. These alterations were correlated with a significant increase of tau pathology (**Fig. 7a**; **Figs. 2** and **3**). We also detected significant increases in the immunoreactivity of ATF4 and CHOP in human AD cases with moderate (Braak III-IV) and severe (Braak V-VI) tau pathology **(Fig. 8).** Using the

Western blot assay, we found that the protein expression of TFEB was significantly decreased in human AD compared to control cases (**Supplementary Figs. 6d** and **6h**), and in PS19;*Wfs1*$^{+/-}$ and PS19;*Wfs1*$^{-/-}$ compared to PS19 mice (**Supplementary Figs. 6c** and **6g**). We find that at the bulk level, however, significant differences of ATF4 and CHOP in PS19;*Wfs1*$^{+/-}$ and PS19;*Wfs1*$^{-/-}$ compared to PS19 mice are diminished, with ATF4 protein levels significantly increasing in PS19;*Wfs1*$^{+/-}$ and a trend of increase in *PS19;Wfs1*$^{-/-}$ mice when compared to *PS19* mice (**Supplementary Figs. 6a** and **6e**)**.** No statistically significant increases were observed for CHOP (**Supplementary Figs. 6b** and **6f**)**,** further suggesting the effects of WFS1 deficiency may be cellular and regional specific in AD. In addition, there is no significant difference in the expression of ATF4, CHOP, p62, CTSD or TFEB between *Wfs1*$^{+/-}$, *Wfs1*$^{-/-}$ and WT controls (**Supplementary Fig. 7**), suggesting WFS1 deficiency will not impact chronic ER stress or the ALP in WT control mouse brains. Furthermore, we found that the overexpression of WFS1 using AAV9-CMV-hWFS1 significantly reduced chronic ER stress-associated ATF4 and CHOP proteins, the p62 puncta formation, and tau pathology (**Figs. 7k-p**), while increasing the immunoreactivity of CTSD and TFEB (**Figs. 7q-t**) in PS19 mice. These results suggest that chronic ER UPR and the downstream impairment of ALP contribute to the increased tau pathology induced by WFS1 deficiency, and WFS1 can inhibit tau pathology via the regulation of this mechanism.

Discussion

WFS1 has been extensively studied for its role in Wolfram syndrome [58, 73]. We now reveal a novel function of WFS1—that is, the involvement in the development and progression of tau pathology and neurodegeneration. Taken together, our study identifies WFS1-expressing EX neurons are accumulated with pathological tau, and the mRNA and protein levels of WFS1 were

significantly reduced at early Braak stages of human AD. WFS1 is also highly expressed in other brain regions such as hippocampal CA1, striatum and olfactory bulb. Tau pathology was indeed found in hippocampal CA1 EX neurons in our mouse model (**Supplementary Fig. 8)**, indicating WFS1-expressing cells in CA1 are vulnerable to tau pathology, too. Although there are a lot of WFS1-expressing cells in mouse striatum and olfactory bulb, we did not find obvious tau pathology in those regions (**Supplementary Fig. 8**). Even within the most vulnerable region of EC, we find only a subpopulation of WFS1-expressing EX neurons are vulnerable to tau pathology, suggesting other factors may also contribute to the observed selective vulnerability. This provides further evidence of selective cellular and regional vulnerability to tau pathology in excitatory neurons and the EC layer-II of AD. We also find a significant increase of WFS1 in GFAP-positive astrocytes, which do not show tau pathology, in human AD compared to controls (**Supplementary Fig. 9**). This suggests that astrocytes might upregulate WFS1 to inhibit tau aggregation or promote tau degradation. On the other hand, in *drosophila*, a reduction of *wfs1* in both astroglia and neurons cause neurodegeneration and shorter lifespans when compared to reductions of *wfs1* in neurons alone [61]. These results and our own suggest a critical role for astrocytes may also exist in the presence of altered levels of *wfs1* and that the presence of *wfs1* in both neurons and astrocytes may play a critical role in neurodegeneration and disease progression. The role of astrocytic WFS1 in AD and other neurodegenerative diseases will be further investigated in future studies.

WFS1 deficiency is associated with the development and progression of tau pathology, neurodegeneration and cognitive deficits, whereas increased WFS1 significantly reduces the tau pathology and neurodegeneration in PS19 mice, probably due to the regulation of chronic ER UPR (i.e., ATF4-CHOP-mediated apoptotic pathway) and the downstream ALP. Both ER stress and autophagy have been found to play important roles in neurodegenerative diseases including AD

[21, 49]. Chronic ER stress and ALP dysfunction impair the degradation and clearance of pathologic tau [21, 49]. Inhibiting chronic ER stress or enhancing the ALP can ameliorate the tau pathology and neurodegeneration [1, 7, 21, 25, 34, 49, 57, 60]. Identification of the protective role of WFS1 in reducing the tau pathology and neurodegeneration could point to a novel therapeutic approach for tau-related neurodegenerative diseases. Importantly, we observe significant reductions of WFS1 in human cases with non-AD tauopathy (FTLD-Tau) and non-tauopathy proteinopathies (FTLD-TDP, and DLBD) by Western blot (**Fig. 1h**) and by IF (**Supplementary Fig.2**). These results suggest a critical role for WFS1 may indeed be applicable to several neurogenerative diseases associated with protein aggregation, possibly by altering the ALP or any upstream key players that modulate protein clearance and degradation.

The defects of the ALP have been found to be strongly associated with protein aggregates in late-onset neurodegenerative diseases such as AD, Parkinson's disease, FTLD, Huntington disease and amyotrophic lateral sclerosis [4, 50]. Promoting the clearance of these aggregates in the brain is typically associated with improvement of symptoms [74]. Thus, enhancing the activity of the ALP is an appealing therapeutic intervention [4, 47, 50]. TFEB, a master regulator of ALP [63, 65], has been widely demonstrated to ameliorate pathology in these diseases [4, 10, 47, 50]. In particular, TFEB has been shown to enhance astroglial uptake of extracellular tau species and reduces tau spreading [46], while its loss of function exacerbates tau pathology and spreading [72]. In this study, we found TFEB is significantly reduced in human early AD, which is correlated with reduced WFS1 and increased tau pathology. Furthermore, WFS1 deficiency reduces the level of TFEB and increases tau pathology and neurodegeneration, while overexpression of WFS1 increases the level of TFEB and protects the vulnerable neurons from tau accumulation and

neurodegeneration in PS19 mice. These data strengthen the hypothesis that enhancing the TFEB-mediated ALP can be an effective therapeutic against AD and other neurodegenerative diseases.

Single-nucleus (sn) RNA-Seq and spatially resolved transcriptomics (ST) like 10x Genomics Visium technology allows us to understand the molecular mechanisms underlying AD, especially the cellular and regional vulnerability, at the system level [9, 19, 22, 42, 48]. In this study, we analyze snRNA-Seq and spatial transcriptomic datasets from human postmortem AD and control brains and find that ER stress and autophagy pathways are enriched in WFS1-high expressing EX neurons and in layer II of the EC in human early AD. The impact of applying state-of-art techniques such as snRNA-Seq and spatial transcriptomics to study the molecular mechanisms underlying AD pathogenesis were further strengthened by follow-up animal studies that also demonstrated chronic ER stress and downstream ALP dysfunction could indeed contribute to the vulnerability of WFS1-expressing EX neurons in tau transgenic mice and human AD at early Braak stages.

Recently, Delpech *et al*. has identified that pathologic tau is accumulated in $WFS1^{+}$ EX neurons in EC layer-II, and the number of these neurons is reduced in human AD with late Braak stages [12]. This is consistent with our findings that WFS1-expressing EX neurons are vulnerable to tau pathology. They also demonstrate the presence of WFS1 in EX neurons of EC layer-II is linked to tau propagation from this layer to the CA1 region of mouse hippocampus [12], implicating another critical role of WFS1 in AD and other tau related diseases (tauopathies). These findings are in line with our evidence of tau interacting with WFS1 at the ER and synapse (**Figure 5**), indicating a possible takeover of WFS1 protective functions in the presence of pathological tau may be critical to disease onset and progression. Further research is required to truly determine whether the deficiency of WFS1 mediates tau dysfunction or if pathological tau may overload the

ER UPR and ALP pathway and in turn overrun WFS1's protective function using human-based models.

Propagation of tau between neurons is considered to play an important role in the neuronal and regional vulnerability of AD and tauopathies [23, 26, 56]. Interestingly, we observed pathologic tau was not only accumulated in superficial layers of the EC but also in deep layers of the cortex in *Wfs1*-deficient PS19 mice, while age-matched PS19 mice did not show the accumulation of pathologic tau in deep layers of the cortex. Furthermore, overexpression of human WFS1 reduced the aggregation and propagation of DS9 tau seeds *in vitro*. These results suggest that WFS1 may play an important role in the propagation of aggregated tau protein between neurons. Future *in vivo* studies are warranted to detect and quantitate tau spread in mouse models in order to conclude how WFS1 levels may mitigate tau spread. Recent findings also support a role for microglia and astrocytes in the uptake and propagation of pathological tau [2, 5, 46, 59]. In particular, TFEB has been found to enhance astroglial uptake of extracellular tau species and reduce tau propagation [46]. Although glial cells are not a focus of this current work, we did observe increases in GFAP staining and hypertrophy (**Fig. 3**) as a result of WFS1 deficiency, indicating increases in astrogliosis in PS19 mice. On the other hand, overexpression of human WFS1 reduces astrogliosis (**Fig. 4**). The role of astrocytes in WFS1 deficiency-mediated tau aggregation and propagation needs to be further investigated in the future.

There are several limitations in this study. First, we investigated the role of ubiquitous knockout or overexpression of WFS1 in the development of tau pathology and neurodegeneration. Therefore, we cannot distinguish the role of WFS1 from the central nervous system or the periphery. The role of brain- and/or cell-type-specific WFS1 on tau pathogenesis are warranted in the future. Second, we used EC-tau and PS19 tau transgenic mouse models in this study. EC-tau

and PS19 mice are widely used as tau animal models with spatiotemporal distribution of tau pathology, gliosis, neuronal loss and cognitive deficits at different ages, which resemble AD-like pathology [11, 18, 41, 45, 76]. The expression of human mutant tau in these mice, however, is several folds higher than that of the endogenous mouse protein. Also, no tau mutations have been identified in AD so far. Therefore, future studies would benefit from using humanized tau models with physiological levels of human wild-type tau in order to validate our findings. Third, given the sex-specific differential response to AD pathology that has been implicated in the pathogenesis of sex dimorphism in AD [13, 48], we will further determine if the protective role of WFS1 on tau pathology and neurodegeneration is sex-dependent. Fourth, we observed decreased protein levels of PSD95 in WFS1 deficient models, which suggests synaptic function may be impaired. Future experiments, such as LTP measurements, are needed to assay for synaptic function in order to determine if WFS1 deficiency alters synaptic function. Finally, the homozygous *Wfs1* KO mice (*Wfs1*$^{-/-}$) have been reported to show a full penetrance and more pronounced phenotype than heterozygous mutants (*Wfs1*$^{+/-}$)[27, 28, 69]. In this study, we observed more severe phenotypes in the homozygote (*PS19;Wfs1*$^{-/-}$) than in the heterozygote (*PS19;Wfs1*$^{+/-}$) in the presence of the PS19 transgene, including the pronounced postsynaptic degeneration (**Figs. 3g** and **3h**), apoptotic cell death (**Figs. 3i** and **3j**), and spatial learning and memory deficits (**Figs. 3k-m**). We also found, however, less astrogliosis (**Figs. 3e** and **3f**) in the homozygote than in the heterozygote in the presence of the PS19 transgene. The reason for this opposite difference in astrogliosis is unknown. One possible reason could be that there is a severe loss of functional astrocytes in the homozygote than in the heterozygote mice due to more cell death in the former. The future studies focusing on the function and dysfunction of reactive astrocytes in those mice are warranted.

Currently, there are no effective neuroprotective or disease-altering treatments available for patients with AD. Understanding if and how WFS1 affects selective vulnerability to tau pathology and neurodegeneration in early AD and other Tauopathies may provide significant insights into the molecular mechanisms underlying neurodegeneration and memory deficits in AD, which will aid in the discovery of novel drug targets (such as WFS1 and/or ALP enhancers) aimed at promoting tau degradation and protecting vulnerable neurons and cognition in early AD.

Contributions

H.F. designed and supervised the study, discussed the results, and wrote the paper. S.C., D.A., L.L., and J.L. designed and performed experiments and analyzed the data and helped write the paper. Y.C. generated all the pipelines for analyzing the 10x Genomics Visium datasets. C.W. performed the single-nucleus RNA-Seq analysis. J.F. and O.N.K. performed the behavioral tests. C.M. helped with the imaging data analysis. C.N.G. performed the immuno-electron microscopy. Y.N., N.C.H.V., and L.V. took part in the pilot studies. C.B. and M.W. helped with the PCR. G.E.S., E.B., X.E.F., L.S.H., J.P.V., D.W.S., and T.G.B. prepared and characterized the human brain samples. T.W. performed the MSD assay. P.P., T.G.B., Q.M., J.K., S.K., F.U., and K.E.D. discussed and edited this paper.

Competing interests

All authors declare no competing interests.

Acknowledgements

This work was supported by awards K01-AG056673, R56-AG066782-01 and R01-AG075092-01 (H.F.) from the National Institute on Aging of the National Institutes of Health and the award R01-GM131399 (Q.M.) from the National Institute of General Medical Sciences. The work was also supported by the award of AARF-17-505009 (H.F.) from the Alzheimer's Association, the W81XWH1910309 (H.F.) from the Department of Defense, and the 10x Genomics 2021 Neuroscience Challenge award. Neurobehavioral tests were performed in the Department of Neuroscience Rodent Behavioral Core at Ohio State University, which was supported by NINDS P30NS04578. Some images were taken in the Department of Neuroscience Image Core, which was supported by P30 NS104177. The MSD assay was performed by the Clinical Research Center Analytical & Development Lab at The Ohio State University supported by Award Number UL1TR002733 from the National Center for Advancing Translational Sciences. We sincerely thank Marc Diamond for sharing the RD-P301S-YFP lentivector and DS9 tau cell line, Peter Davies for providing MC1, PHF1, and DA9 tau antibodies, and University of Tartu for sharing the *Wfs1* knockout mice. We also thank Drs. Gail V.W. Johnson, Wai Haung Yu, Eric Klann and Andrea Tedeschi for helpful discussion. We thank the 10x Genomics technical support team for helpful discussions. We also thank Amanda Toland, Pearlly Yan, Tom Liu, Jennifer Mele from the Ohio State University and Amy Wetzel from the Nationwide Children's Hospital for helping with the RNA quality control and the sequencing. The RNA quality control was performed at NCI subsidized shared resource supported by The Ohio State University Comprehensive Cancer Center and the National Institutes of Health under grant number P30 CA016058. We thank Michael Rose and Rebecca Davis at The Ohio State University for preparing the human brain samples. Human de-identified brain tissues were kindly provided by the Banner Sun Health Research Institute Brain and Body Donation Program, supported by NIH grants U24-NS072026 and P30-AG19610 (TGB),

the Arizona Department of Health Services (contract 211002, Arizona Alzheimer's Research Center), the Arizona Biomedical Research Commission (contracts 4001, 0011, 05-901 and 1001 to the Arizona Parkinson's Disease Consortium) and the Michael J. Fox Foundation for Parkinson's Research as well as the Buckeye Brain Bank and the Buckeye Biospecimen Repository at the Ohio State University, and the New York Brain Bank at Columbia University Irving Medical Center supported by the Taub Institute and NIH grants P50AG008702 and P30AG066462. This work used the high-performance computing infrastructure at the Ohio State University.

Table 1. Post-mortem Case Demographics.

Case ID	Sex	Age (yr)	AD	Other NDs	Amyloid Thal phase (A)	Braak NFT stage (B)	CERAD neuritic plaque score (C)	Section type	Use	Source
1	M	89	No	No	1	1	1	FFPE	IF	BH
2	M	65	No	No	0	1	0	FFPE	IF	BH
3	M	73	No	No	0	1	0	FFPE	IF	BH
4	M	82	No	No	0	1	0	FFPE	IF	BH
5	M	78	No	No	0	1	0	FFPE	IF	BH
6	M	86	Yes	No	3	2	3	FFPE, FR	IF, WB	BH
7	M	82	Yes	No	3	2	3	FFPE, FR	IF, WB	BH
8	M	78	Yes	No	3	2	3	FFPE	IF	BH
9	M	86	Yes	No	3	2	3	FFPE, FR	IF, WB	BH
10	M	80	Yes	No	2	2	2	FFPE	IF	BH
11	M	78	Yes	No	3	3	3	FFPE	IF	BH
12	M	87	Yes	No	3	3	3	FFPE	IF	BH
13	M	71	Yes	No	3	3	3	FFPE	IF	BH
14	M	76	Yes	No	3	3	3	FFPE	IF	BH
15	M	78	Yes	No	3	3	3	FFPE	IF	BH
16	M	82	No	No	0	1	0	FR	IF, Visium	BH

17	M	72	No	No	0	1	0	FR	IF, Visium	BH
18	M	86	Yes	No	3	2	3	FR	IF, Visium	BH
19	M	75	No	No	1	1	0	FR	IF, WB	CUIMC
20	F	54	No	No	0	1	0	FR	IF, Duolink	CUIMC
21	M	62	No	No	0	1	0	FR	IF, Duolink	CUIMC
22	M	66	No	No	0	1	0	FR	IF, Duolink	CUIMC
23	F	89	Yes	No	2	2	2	FR	IF, Duolink	CUIMC
24	M	89	Yes	No	2	2	1	FR	IF, Duolink	CUIMC
25	M	88	Yes	No	3	3	2	FR	IF, Duolink	CUIMC
26	M	73	Yes	No	3	3	3	FR	IF, Duolink	CUIMC
27	F	89	Yes	No	3	3	3	FR	IF, Duolink	CUIMC
28	M	89	Yes	No	3	2	2	FR	IF, Visium, Duolink	CUIMC
29	M	58	No	No	0	1	0	FR	WB	OSU
30	M	87	No	No	0	1	0	FR	WB	OSU
31	M	78	No	No	0	1	0	FR	WB	OSU
32	M	77	No	No	0	1	0	FR	WB	OSU
33	F	73	No	No	0	1	0	FR	WB	OSU
34	M	71	Yes	No	2	2	2	FR	WB	OSU
35	M	90	Yes	No	2	2	2	FR	WB	OSU
36	M	72	No	DLBD	NA	NA	NA	FR	IF, WB	CUIMC
37	M	65	No	DLBD	NA	NA	NA	FR	IF, WB	CUIMC
38	F	69	No	DLBD	NA	NA	NA	FR	IF, WB	CUIMC
39	M	58	No	FTLD-Tau	NA	NA	NA	FR	IF, WB	OSU
40	M	57	No	FTLD-Tau	NA	NA	NA	FR	IF, WB	CUIMC
41	F	77	No	FTLD-Tau	NA	NA	NA	FR	IF, WB	CUIMC
42	F	87	No	FTLD-TDP	NA	NA	NA	FR	IF, WB	OSU
43	F	54	No	FTLD-TDP	NA	NA	NA	FR	IF, WB	CUIMC
44	M	64	No	FTLD-TDP	NA	NA	NA	FR	IF, WB	CUIMC

677

AD, Alzheimer's disease; M, male; F, female; NDs: neurodegenerative diseases including Diffuse Lewy body disease (DLBD), Frontotemporal lobar degeneration with abnormal tau burden (FTLD-Tau), Frontotemporal lobar degeneration with TDP-43 (FTLD-TDP), Parkinson's disease, Vascular dementia, Progressive supranuclear palsy, Hippocampal sclerosis, Dementia lacking distinctive histology, Motor neuron disease, Corticobasal degeneration, Pick's disease, Huntington's disease, Multiple system atrophy, Argyrophilic grain disease, Cerebral white matter rarefaction, and Multiple sclerosis; NA, not available; FR, frozen section; FFPE, formalin-fixed paraffin-embedded section; IF, immunofluorescence staining; BH, Banner Sun Health Research Institute; CUIMC, Columbia University Irving Medical Center; OSU, Ohio State University. All samples are classified according to the ABC scoring method described in the National Institute of Aging-Alzheimer's Association guidelines for the neuropathologic assessment of AD (NIA-AA AD)[51].

Figures and legends

Fig. 1. WFS1 is significantly reduced in EC-tau mice, human AD and other types of proteinopathies. (**a** & **b**) Representative confocal images of $WFS1^+$ cells (red), conformational changed tau stained by MC1 (green), and their colocalization (yellow) in EC-tau mice at 14 mo (months) **(a),** and AD (Braak stage V) with severe tau pathology (**b**). The nuclei were stained by DAPI (blue). Scale bar, 50 μm. (**c** & **d**) Representative images of WFS1 (red) expressed in the EC of EC-tau mice at 14 mo and 30+ mo (**c**), and the EC of control (CT) cases with very minor tau pathology due to aging and AD cases (Braak V-VI) with severe tau pathology (**d**). Scale bar, 100 μm. (**e** & **f**) The number of $WFS1^+$ cells in the medial EC (MEC) of EC-tau mice at different ages (**e**), and in the EC of human CT, AD (Braak III-IV) and AD (Braak V-VI) cases (**f**). $^{**}P < 0.01$ *vs* 14-month-old EC-tau mice (n=5 mice/group) (**e**) or CT cases (n=5 cases/group) (**f**) (Mann-Whitney test). (**g**) Total protein extracts from human CT and AD (Braak III-IV) cases were subjected to Western blot (WB) assay and probed with specific rabbit anti-WFS1 (green) and mouse anti-β-tubulin (red, internal control) antibodies. Lane 1 (PM): red, LiCor protein markers. (h) Total protein extracts from human CT, FTLD-Tau, FTLD-TDP, and DLBD (n=3 cases/group) were subjected to WB assay probed with rabbit anti-WFS1 (green) and mouse anti-GAPDH (red). (**i**) Quantitation of the protein expression of WFS1 and β-tubulin in panel g. The ratio of WFS1/β-tubulin was compared between human CT and AD. $^{*}P < 0.05$ *vs* CT (n=5 cases/group, Mann-Whitney test). (**j**) Quantitation of the protein expression of WFS1 and GAPDH in panel h. The ratio of WFS1/GAPDH was compared between human CT and FTLD-Tau, FTLD-TDP, and DLBD. $^{*}P < 0.05$, $^{***}P < 0.001$ *vs* CT (n=3 cases/group, unpaired *t*-test).

Fig. 2. Whole-body WFS1 knockout increases phosphorylated tau in the cortex of PS19 tau mice. (**a**) The total protein, sarkosyl-soluble (SS) and sarkosyl-insoluble (SI) lysates from mouse cortex at 8.7 mo were subjected to WB assay and probed with specific rabbit anti-WFS1 (green), mouse anti-β-tubulin (red, internal control), mouse anti-PHF1 (red), and rabbit anti-TauC antibodies. PM, LiCor protein markers. PHF1 in SS lysate and SI lysate share the same PM. TauC in SS lysate and SI lysate also share the same PM. (**b-d**) Quantitation of the protein expression in panel A. The ratios of WFS1/β-tubulin and PHF1/TauC were compared. $^{*}P < 0.05$, $^{***}P < 0.001$ *vs* PS19 (n=4 mice/group). (**e-h**) The total tau and pT231 tau in the SS and SI lysates were measured using the MSD Phospho(Thr231)/Total Tau ELISA Kit. $^{**}P < 0.01$ *vs* PS19 (n=6-12 mice/group).

Fig. 3. Increased tau pathology in whole-body WFS1 knockout coincides with astrogliosis, postsynaptic degeneration, apoptosis and cognitive deficits in PS19 tau mice. (**a**) Representative images of the immunoreactivity of conformational changed tau stained by MC1 (green) and WFS1 (red) in the EC of PS19, *PS19;Wfs1*$^{+/-}$, and *PS19;Wfs1*$^{-/-}$ mice at 8.7 mo. The nuclei were stained by DAPI (blue). Scale bar, 500 μm. Inset images are high magnification images in the superficial layer (yellow box) and the deep layer (white box) of EC. Scale bar, 30 μm. (**b**) Quantitation of MC1^{+} cells shown in panel A. (**c**) Representative images of the immunoreactivity of MC1 (green) and excitatory neuronal marker, SATB2 (red), in the EC of PS19, *PS19;Wfs1*$^{+/-}$, and *PS19;Wfs1*$^{-/-}$ mice at 8.7 mo. Scale bar, 65 μm. (**d**) Quantitation of SATB2^{+} cells shown in panel c. (**e**, **g**, **i**) Representative images of the immunoreactivity of GFAP (astrocyte marker) (**e**), PSD95 (postsynaptic marker) (**g**), and the measurement of apoptosis using the TUNEL assay (**i**) in the EC of PS19, *PS19;Wfs1*$^{+/-}$, and *PS19;Wfs1*$^{-/-}$ mice at 8.7 mo. Scale bars are 200 μm for (**e**) and (**i**), 100 μm for (**g**), and 30 μm for all the insets. (**f**, **h**, **j**) The mean intensity of GFAP (**f**) and PSD95 (**h**) and the number of TUNEL^{+} cells (**j**) were quantitated by ImageJ. **P* < 0.05, ***P* < 0.01 *vs* PS19 or *vs PS19;Wfs1*$^{+/-}$ (n=6-9 mice/group, Mann-Whitney test). Nuclei were stained by DAPI. (**k**) Y-maze test was utilized to investigate spatial working memory in mice with different genotypes. The percentage of spontaneous alternation was calculated as the actual alternations divided by the possible alternation (total arm entries − 2) × 100. The mice with total entries ≤ 2 were excluded from analysis. **P* < 0.05 *vs PS19;Wfs1*$^{+/-}$; ***P* < 0.01, ****P* < 0.001 *vs* PS19 (n=8-22 mice/group, Mann-Whitney test). (**l-m**) Spatial learning and memory was also measured by Barnes maze test. The latency to goal perimeter of escape hole during training session (**l**) and the time spent in Q3 (**m**) (the quadrant where the escape hole was previously located) in the probe test were compared between different genotypes. **P* < 0.05, ***P* < 0.01, and ****P* < 0.001 vs PS19 (**l**) or **P* < 0.05 vs PS19 or PS19;*Wfs1*$^{+/-}$ (**m**) (n=8-21 mice/group, a mixture of male and female mice, Mann-Whitney test).

Fig. 4. Overexpression of human WFS1 attenuates tau pathology, astrogliosis, postsynaptic degeneration and apoptosis in PS19 tau mice. (**a**) Representative tile images of the immunoreactivity of GFAP (green), MC1 (red), WFS1 (white), and PSD95 (red) (**c**), and the measurement of apoptosis using the TUNEL assay (red) (**e**) 3 months after the stereotaxic microinjection of 0.5 μl of AAV9-CMV-hWFS1 or control AAV9 into the EC and hippocampus of 8-mo-old PS19 mice, respectively. The nuclei were stained by DAPI. (**b**, **d**, **f**) The number of MC1-positive cells (**b**), the mean intensity of GFAP (**b**) and PSD95 (**d**), and TUNEL^{+} cells (**f**) in the EC were compared between mice injected with AAV9-CMV-hWFS1 or control AAV9 using ImageJ. ***P* < 0.01, ****P* < 0.001 *vs* Control AAV9 (n=4 mice x 2 sections/group, Mann-Whitney test). Scale bar, 500 μm.

Fig. 5. WFS1 interacts with pathologic tau protein and reduces tau seeding. Representative immuno-electron microscopy images of the distribution of WFS1 (6-nm gold particles, red arrows) and human pathological tau stained by MC1 (10-nm gold particles, white arrows) in the endoplasmic reticulum (ER) (**left panel a**) and synapse (**right panel a**) of 9.5-month-old PS19 mice. PSD: post-synaptic density; SVs: synaptic vesicles. (**b** & **d**) Visualization of the protein interaction between pathologic tau and WFS1 in EC-tau and *Wfs1*$^{-/-}$ mice as well as human control and AD cases using the Duolink PLA assay. Mouse or human frozen brain sections were fixed and sequentially stained with primary rabbit anti-WFS1 and mouse anti-AT8 pTau antibodies. The next day, the sections were washed and incubated with a pair of PLA probes according to the fluorescence protocol provided in the Red Starter Kit. The red single dots around the nucleus (blue) imaged by confocal microscopy indicate the protein-protein interaction of WFS1 with pathological

tau AT8 in mouse (**b**) and human frozen brain sections (**d**). (**c** & **e**) The red dots per cell were compared using nonparametric Mann-Whitney test. ***P<0.001 (n=43-57 and 59-60 neurons each group in **b** and **d**, respectively). Wfs1 knockout (*Wfs1*$^{-/-}$) was used as a negative control. The reduction of red dot numbers in late AD may be due to the neuronal loss. Scale bar, 5 µm. (**f**) Overexpression of human WFS1 reduces DS9 tau seeding. SH-SY5Y cells stably expressing *P301S* mutant tau were transduced with different concentrations of control or WFS1 lentiviruses for 24 h and then treated with DS9 tau seeds. Representative live images of tau aggregates (green puncta) from three independent experiments were taken 24 hours after the incubation of DS9 tau seeds. Scale bar, 50 µm. (**g**) Cells were fixed with 4% PFA and stained with rabbit anti-WFS1 antibody. Most large tau aggregates were found in cells without overexpression of WFS1 (arrowheads). Scale bar, 50 µm. (**h**) Comparison of the area of tau aggregates in control and WFS1 lentivirus-treated conditions. ***P < 0.001 (Mann-Whitney test).

Fig. 6. Analysis of snRNA-Seq and spatial transcriptomic datasets from human control and early AD cases. (**a** & **b**) The expression level of WFS1 mRNA in excitatory (EX) neurons of human cases with differential tau pathology and the enriched signaling pathways in WFS1-high EX neurons at early AD. The snRNA-Seq data (GSE147528) from human EC at Braak stage 0 control), 2, and 6 was used for this analysis. (**a**) Violin plot shows the expression of WFS1 in EX neurons (> WFS1 mean expression value in each stage) at different Braak stages. ***P < 0.001 *vs* stage 0 or stage 2 (Wilcoxon rank sum test with Bonferroni correction). (**b**) Differentially expressed genes were assessed with the Seurat FindMarkers function with a log-fold-change threshold of 0.25. Bonferroni-adjusted p-values were used to determine significance at an FDR < 0.05. Dot plot shows top 5 enriched GO: biological process terms from the differentially expressed genes between WFS1-high (> 2x mean) vs WFS1-low (< 2x mean) EX neurons in stage 2 dataset. Each dot is colored by the Benjamini-Hochberg adjusted p-value. The dot size is scaled by the number of overlapping genes with the related GO terms. The x-axis is scaled by the ratio between the overlapping count and the total number of genes of the term. Gene set enrichment analysis was performed using the Enrichr web server. (**c**) Brain samples (middle temporal gyrus, MTG) from a 72-year-old control male (top) and an 89-year-old AD male (bottom, Braak stage-III) were characterized by 10x Genomics Visium spatial transcriptomics. The figures in the first column show the spatial localization of identified 14 clusters in control (7 clusters) and AD (7 clusters). The middle four feature plots visualize WFS1 (gradient blue) and MAPT (gradient red) gene expression in control and AD. The color legends of the feature plots indicate the log-scaled normalized expression value. The right two figures show the distribution of WFS1 and MAPT gene co-expressed spots (purple) with respect to control and AD. Clustering results were generated by Seurat (v3.2.2). All figures were generated by 10x Genomics Loupe Browser (v 4.1.0). (**d**) Differentially expressed genes were assessed with the Seurat FindMarkers function with a log-fold-change threshold of 0.1. Bonferroni-adjusted p-values were used to determine significance at an FDR < 0.05. Dot plot shows 5 significantly enriched GO: biological process terms from the differentially expressed genes in the WFS1^{+}/AT8 pTau^{+} spots *vs* adjacent spots in Layer 2 of AD brain samples, which was determined by IF staining of adjacent human brain sections (10 µm apart) with WFS1 and AT8 antibodies. Each dot is colored by the Benjamini-Hochberg adjusted p-value. The dot size is scaled by the number of overlapping genes with the related GO terms. Gene set enrichment analysis was performed using the Enrichr web server.

Fig. 7. WFS1 deficiency alters key proteins associated with chronic ER stress and ALP in PS19 mice, while WFS1 overexpression reverses these changes. (**a-i**) Representative images of the immunoreactivity of p62 (green) and MC1 (red), ATF4 (red), CHOP (red), CTSD (green), and

TFEB (green) in the EC of 8.7-mo-old *PS19* mice and *PS19;Wfs1*$^{+/-}$ mice. The nuclei were co-stained by DAPI (blue). Inset images: p62 (green), ATF4 (red), CHOP (red), CTSD (green), TFEB (green). Scale bars are 65 µm for tiles images, and 5 µm for insets. The number of cells with aggregated p62 puncta (**b**), the mean intensity of ATF4 (**d**), CHOP (**f**), CTSD (**h**), and TFEB (**j**) were compared using ImageJ. ***P* < 0.01 *vs* PS19 mice (n=6-12 mice/group, Mann-Whitney test). (**k-s**) Representative images of the immunoreactivity of p62 (green) and MC1 (red), ATF4 (red) CHOP (red), CTSD (green), and TFEB (green) 3 months after the stereotaxic microinjection of 0.5 µl of AAV9-CMV-hWFS1 or control AAV9 into the EC of 8-mo-old PS19 mice. The number of cells with aggregated p62 puncta (**l**) and the mean intensity of ATF4 (**n**), CHOP (**p**), CTSD (**r**), and TFEB (**t**) were compared using ImageJ. **P* < 0.05, ****P* < 0.001 vs Control AAV9 (n=3 mice x 2 sections/group, Mann-Whitney test). Scale bars, 65 µm.

Fig. 8. Upregulated level of ATF4 and CHOP in human AD. (**a**) Representative images of ATF4 (top) and CHOP (bottom) in CT, AD (Braak III-IV), and AD (Braak V-VI) postmortem human brain. (**b & c**) Mean intensity of ATF4 (**b**) and CHOP (**c**) were compared between CT, AD (Braak III-IV), and AD (Braak V-VI). ****P* < 0.001 vs CT (n=3 cases, 5 images/case, Mann-Whitney test). Scale bars, 100 µm, and 10 µm for insets.

References

1 Abisambra JF, Jinwal UK, Blair LJ, O'Leary JC, 3rd, Li Q, Brady S, Wang L, Guidi CE, Zhang B, Nordhues BA, et al. (2013) Tau accumulation activates the unfolded protein response by impairing endoplasmic reticulum-associated degradation. J Neurosci 33: 9498-9507 Doi 10.1523/JNEUROSCI.5397-12.2013

2 Asai H, Ikezu S, Tsunoda S, Medalla M, Luebke J, Haydar T, Wolozin B, Butovsky O, Kugler S, Ikezu T (2015) Depletion of microglia and inhibition of exosome synthesis halt tau propagation. Nat Neurosci 18: 1584-1593 Doi 10.1038/nn.4132

3 Beach TG, Adler CH, Sue LI, Serrano G, Shill HA, Walker DG, Lue L, Roher AE, Dugger BN, Maarouf C, et al. (2015) Arizona Study of Aging and Neurodegenerative Disorders and Brain and Body Donation Program. Neuropathology 35: 354-389 Doi 10.1111/neup.12189

4 Boland B, Yu WH, Corti O, Mollereau B, Henriques A, Bezard E, Pastores GM, Rubinsztein DC, Nixon RA, Duchen MR, et al. (2018) Promoting the clearance of neurotoxic proteins in neurodegenerative disorders of ageing. Nat Rev Drug Discov 17: 660-688 Doi 10.1038/nrd.2018.109

5 Bolos M, Llorens-Martin M, Jurado-Arjona J, Hernandez F, Rabano A, Avila J (2016) Direct Evidence of Internalization of Tau by Microglia In Vitro and In Vivo. J Alzheimers Dis 50: 77-87 Doi 10.3233/JAD-150704

6 Braak H, Braak E (1991) Neuropathological stageing of Alzheimer-related changes. Acta Neuropathol 82: 239-259 Doi 10.1007/BF00308809

7 Cagalinec M, Liiv M, Hodurova Z, Hickey MA, Vaarmann A, Mandel M, Zeb A, Choubey V, Kuum M, Safiulina D, et al. (2016) Role of Mitochondrial Dynamics in Neuronal Development: Mechanism for Wolfram Syndrome. PLoS Biol 14: e1002511 Doi 10.1371/journal.pbio.1002511

8 Chen S, Chang Y, Li L, Acosta D, Morrison C, Wang C, Julian D, Hester ME, Serrano GE, Beach TG, et al. (2021) Spatially resolved transcriptomics reveals unique gene signatures associated with human temporal cortical architecture and Alzheimer's pathology. 2021.2007.2007.451554 Doi 10.1101/2021.07.07.451554 %J bioRxiv

9 Chen WT, Lu A, Craessaerts K, Pavie B, Sala Frigerio C, Corthout N, Qian X, Lalakova J, Kuhnemund M, Voytyuk I, et al. (2020) Spatial Transcriptomics and In Situ Sequencing to Study Alzheimer's Disease. Cell 182: 976-991 e919 Doi 10.1016/j.cell.2020.06.038
10 Cortes CJ, La Spada AR (2019) TFEB dysregulation as a driver of autophagy dysfunction in neurodegenerative disease: Molecular mechanisms, cellular processes, and emerging therapeutic opportunities. Neurobiol Dis 122: 83-93 Doi 10.1016/j.nbd.2018.05.012
11 de Calignon A, Polydoro M, Suarez-Calvet M, William C, Adamowicz DH, Kopeikina KJ, Pitstick R, Sahara N, Ashe KH, Carlson GA, et al. (2012) Propagation of tau pathology in a model of early Alzheimer's disease. Neuron 73: 685-697 Doi 10.1016/j.neuron.2011.11.033
12 Delpech JC, Pathak D, Varghese M, Kalavai SV, Hays EC, Hof PR, Johnson WE, Ikezu S, Medalla M, Luebke JI, et al. (2021) Wolframin-1-expressing neurons in the entorhinal cortex propagate tau to CA1 neurons and impair hippocampal memory in mice. Sci Transl Med 13: eabe8455 Doi 10.1126/scitranslmed.abe8455
13 Fisher DW, Bennett DA, Dong H (2018) Sexual dimorphism in predisposition to Alzheimer's disease. Neurobiol Aging 70: 308-324 Doi 10.1016/j.neurobiolaging.2018.04.004
14 Fonseca SG, Fukuma M, Lipson KL, Nguyen LX, Allen JR, Oka Y, Urano F (2005) WFS1 is a novel component of the unfolded protein response and maintains homeostasis of the endoplasmic reticulum in pancreatic beta-cells. J Biol Chem 280: 39609-39615 Doi 10.1074/jbc.M507426200
15 Fonseca SG, Ishigaki S, Oslowski CM, Lu S, Lipson KL, Ghosh R, Hayashi E, Ishihara H, Oka Y, Permutt MA, et al. (2010) Wolfram syndrome 1 gene negatively regulates ER stress signaling in rodent and human cells. J Clin Invest 120: 744-755 Doi 10.1172/JCI39678
16 Fredriksson S, Gullberg M, Jarvius J, Olsson C, Pietras K, Gustafsdottir SM, Ostman A, Landegren U (2002) Protein detection using proximity-dependent DNA ligation assays. Nat Biotechnol 20: 473-477 Doi 10.1038/nbt0502-473
17 Fu H, Hardy J, Duff KE (2018) Selective vulnerability in neurodegenerative diseases. Nat Neurosci 21: 1350-1358 Doi 10.1038/s41593-018-0221-2
18 Fu H, Hussaini SA, Wegmann S, Profaci C, Daniels JD, Herman M, Emrani S, Figueroa HY, Hyman BT, Davies P, et al. (2016) 3D Visualization of the Temporal and Spatial Spread of Tau Pathology Reveals Extensive Sites of Tau Accumulation Associated with Neuronal Loss and Recognition Memory Deficit in Aged Tau Transgenic Mice. PLoS One 11: e0159463 Doi 10.1371/journal.pone.0159463
19 Fu H, Possenti A, Freer R, Nakano Y, Hernandez Villegas NC, Tang M, Cauhy PVM, Lassus BA, Chen S, Fowler SL, et al. (2019) A tau homeostasis signature is linked with the cellular and regional vulnerability of excitatory neurons to tau pathology. Nat Neurosci 22: 47-56 Doi 10.1038/s41593-018-0298-7
20 Fu H, Rodriguez GA, Herman M, Emrani S, Nahmani E, Barrett G, Figueroa HY, Goldberg E, Hussaini SA, Duff KE (2017) Tau Pathology Induces Excitatory Neuron Loss, Grid Cell Dysfunction, and Spatial Memory Deficits Reminiscent of Early Alzheimer's Disease. Neuron 93: 533-541 e535 Doi 10.1016/j.neuron.2016.12.023
21 Fujita E, Kouroku Y, Isoai A, Kumagai H, Misutani A, Matsuda C, Hayashi YK, Momoi T (2007) Two endoplasmic reticulum-associated degradation (ERAD) systems for the novel variant of the mutant dysferlin: ubiquitin/proteasome ERAD(I) and autophagy/lysosome ERAD(II). Hum Mol Genet 16: 618-629 Doi 10.1093/hmg/ddm002
22 Grubman A, Chew G, Ouyang JF, Sun G, Choo XY, McLean C, Simmons RK, Buckberry S, Vargas-Landin DB, Poppe D, et al. (2019) A single-cell atlas of entorhinal cortex from individuals with Alzheimer's disease reveals cell-type-specific gene expression regulation. Nat Neurosci 22: 2087-2097 Doi 10.1038/s41593-019-0539-4
23 Guo JL, Narasimhan S, Changolkar L, He Z, Stieber A, Zhang B, Gathagan RJ, Iba M, McBride JD, Trojanowski JQ, et al. (2016) Unique pathological tau conformers from Alzheimer's brains transmit tau pathology in nontransgenic mice. J Exp Med 213: 2635-2654 Doi 10.1084/jem.20160833

24 Halliday M, Radford H, Zents KAM, Molloy C, Moreno JA, Verity NC, Smith E, Ortori CA, Barrett DA, Bushell M, et al. (2017) Repurposed drugs targeting eIF2α-P-mediated translational repression prevent neurodegeneration in mice. Brain 140: 1768-1783 Doi 10.1093/brain/awx074
25 Hetz C, Mollereau B (2014) Disturbance of endoplasmic reticulum proteostasis in neurodegenerative diseases. Nat Rev Neurosci 15: 233-249 Doi 10.1038/nrn3689
26 Iba M, McBride JD, Guo JL, Zhang B, Trojanowski JQ, Lee VM (2015) Tau pathology spread in PS19 tau transgenic mice following locus coeruleus (LC) injections of synthetic tau fibrils is determined by the LC's afferent and efferent connections. Acta Neuropathol 130: 349-362 Doi 10.1007/s00401-015-1458-4
27 Ivask M, Hugill A, Koks S (2016) RNA-sequencing of WFS1-deficient pancreatic islets. Physiol Rep 4: Doi 10.14814/phy2.12750
28 Ivask M, Volke V, Raasmaja A, Koks S (2021) High-fat diet associated sensitization to metabolic stress in Wfs1 heterozygous mice. Mol Genet Metab 134: 203-211 Doi 10.1016/j.ymgme.2021.07.002
29 Jack CR, Jr., Bennett DA, Blennow K, Carrillo MC, Dunn B, Haeberlein SB, Holtzman DM, Jagust W, Jessen F, Karlawish J, et al. (2018) NIA-AA Research Framework: Toward a biological definition of Alzheimer's disease. Alzheimers Dement 14: 535-562 Doi 10.1016/j.jalz.2018.02.018
30 Jack CR, Jr., Holtzman DM (2013) Biomarker modeling of Alzheimer's disease. Neuron 80: 1347-1358 Doi 10.1016/j.neuron.2013.12.003
31 Jack CR, Jr., Knopman DS, Jagust WJ, Petersen RC, Weiner MW, Aisen PS, Shaw LM, Vemuri P, Wiste HJ, Weigand SD, et al. (2013) Tracking pathophysiological processes in Alzheimer's disease: an updated hypothetical model of dynamic biomarkers. Lancet Neurol 12: 207-216 Doi 10.1016/S1474-4422(12)70291-0
32 Jicha GA, Bowser R, Kazam IG, Davies P (1997) Alz-50 and MC-1, a new monoclonal antibody raised to paired helical filaments, recognize conformational epitopes on recombinant tau. J Neurosci Res 48: 128-132 Doi 10.1002/(sici)1097-4547(19970415)48:2<128::aid-jnr5>3.0.co;2-e
33 Jucker M, Walker LC (2018) Propagation and spread of pathogenic protein assemblies in neurodegenerative diseases. Nat Neurosci 21: 1341-1349 Doi 10.1038/s41593-018-0238-6
34 Kakiuchi C, Ishiwata M, Hayashi A, Kato T (2006) XBP1 induces WFS1 through an endoplasmic reticulum stress response element-like motif in SH-SY5Y cells. J Neurochem 97: 545-555 Doi 10.1111/j.1471-4159.2006.03772.x
35 Karran E, Mercken M, De Strooper B (2011) The amyloid cascade hypothesis for Alzheimer's disease: an appraisal for the development of therapeutics. Nat Rev Drug Discov 10: 698-712 Doi 10.1038/nrd3505
36 Kawano J, Fujinaga R, Yamamoto-Hanada K, Oka Y, Tanizawa Y, Shinoda K (2009) Wolfram syndrome 1 (Wfs1) mRNA expression in the normal mouse brain during postnatal development. Neurosci Res 64: 213-230 Doi 10.1016/j.neures.2009.03.005
37 Kitamura T (2017) Driving and regulating temporal association learning coordinated by entorhinal-hippocampal network. Neurosci Res 121: 1-6 Doi 10.1016/j.neures.2017.04.005
38 Kitamura T, Pignatelli M, Suh J, Kohara K, Yoshiki A, Abe K, Tonegawa S (2014) Island cells control temporal association memory. Science 343: 896-901 Doi 10.1126/science.1244634
39 Koks S, Soomets U, Paya-Cano JL, Fernandes C, Luuk H, Plaas M, Terasmaa A, Tillmann V, Noormets K, Vasar E, et al. (2009) Wfs1 gene deletion causes growth retardation in mice and interferes with the growth hormone pathway. Physiol Genomics 37: 249-259 Doi 10.1152/physiolgenomics.90407.2008
40 Kuleshov MV, Jones MR, Rouillard AD, Fernandez NF, Duan Q, Wang Z, Koplev S, Jenkins SL, Jagodnik KM, Lachmann A, et al. (2016) Enrichr: a comprehensive gene set enrichment analysis web server 2016 update. Nucleic Acids Res 44: W90-97 Doi 10.1093/nar/gkw377
41 Lasagna-Reeves CA, de Haro M, Hao S, Park J, Rousseaux MW, Al-Ramahi I, Jafar-Nejad P, Vilanova-Velez L, See L, De Maio A, et al. (2016) Reduction of Nuak1 Decreases Tau and

Reverses Phenotypes in a Tauopathy Mouse Model. Neuron 92: 407-418 Doi 10.1016/j.neuron.2016.09.022

42 Leng K, Li E, Eser R, Piergies A, Sit R, Tan M, Neff N, Li SH, Rodriguez RD, Suemoto CK, et al. (2021) Molecular characterization of selectively vulnerable neurons in Alzheimer's disease. Nat Neurosci 24: 276-287 Doi 10.1038/s41593-020-00764-7

43 Li L, Venkataraman L, Chen S, Fu H (2020) Function of WFS1 and WFS2 in the Central Nervous System: Implications for Wolfram Syndrome and Alzheimer's disease. Neurosci Biobehav Rev 118: 775-783 Doi 10.1016/j.neubiorev.2020.09.011

44 Lie PPY, Yang DS, Stavrides P, Goulbourne CN, Zheng P, Mohan PS, Cataldo AM, Nixon RA (2021) Post-Golgi carriers, not lysosomes, confer lysosomal properties to pre-degradative organelles in normal and dystrophic axons. Cell Rep 35: 109034 Doi 10.1016/j.celrep.2021.109034

45 Liu L, Drouet V, Wu JW, Witter MP, Small SA, Clelland C, Duff K (2012) Trans-synaptic spread of tau pathology in vivo. PLoS One 7: e31302 Doi 10.1371/journal.pone.0031302

46 Martini-Stoica H, Cole AL, Swartzlander DB, Chen F, Wan YW, Bajaj L, Bader DA, Lee VMY, Trojanowski JQ, Liu Z, et al. (2018) TFEB enhances astroglial uptake of extracellular tau species and reduces tau spreading. J Exp Med 215: 2355-2377 Doi 10.1084/jem.20172158

47 Martini-Stoica H, Xu Y, Ballabio A, Zheng H (2016) The Autophagy-Lysosomal Pathway in Neurodegeneration: A TFEB Perspective. Trends Neurosci 39: 221-234 Doi 10.1016/j.tins.2016.02.002

48 Mathys H, Davila-Velderrain J, Peng Z, Gao F, Mohammadi S, Young JZ, Menon M, He L, Abdurrob F, Jiang X, et al. (2019) Single-cell transcriptomic analysis of Alzheimer's disease. Nature 570: 332-337 Doi 10.1038/s41586-019-1195-2

49 Meier S, Bell M, Lyons DN, Ingram A, Chen J, Gensel JC, Zhu H, Nelson PT, Abisambra JF (2015) Identification of Novel Tau Interactions with Endoplasmic Reticulum Proteins in Alzheimer's Disease Brain. J Alzheimers Dis 48: 687-702 Doi 10.3233/JAD-150298

50 Menzies FM, Fleming A, Rubinsztein DC (2015) Compromised autophagy and neurodegenerative diseases. Nat Rev Neurosci 16: 345-357 Doi 10.1038/nrn3961

51 Montine TJ, Phelps CH, Beach TG, Bigio EH, Cairns NJ, Dickson DW, Duyckaerts C, Frosch MP, Masliah E, Mirra SS, et al. (2012) National Institute on Aging-Alzheimer's Association guidelines for the neuropathologic assessment of Alzheimer's disease: a practical approach. Acta Neuropathol 123: 1-11 Doi 10.1007/s00401-011-0910-3

52 Morrison JH, Hof PR (2007) Life and death of neurons in the aging cerebral cortex. Int Rev Neurobiol 81: 41-57 Doi 10.1016/S0074-7742(06)81004-4

53 Morrison JH, Hof PR (2002) Selective vulnerability of corticocortical and hippocampal circuits in aging and Alzheimer's disease. Prog Brain Res 136: 467-486 Doi 10.1016/s0079-6123(02)36039-4

54 Moser EI, Kropff E, Moser MB (2008) Place cells, grid cells, and the brain's spatial representation system. Annu Rev Neurosci 31: 69-89 Doi 10.1146/annurev.neuro.31.061307.090723

55 Nakashima A, Cheng SB, Kusabiraki T, Motomura K, Aoki A, Ushijima A, Ono Y, Tsuda S, Shima T, Yoshino O, et al. (2019) Endoplasmic reticulum stress disrupts lysosomal homeostasis and induces blockade of autophagic flux in human trophoblasts. Sci Rep 9: 11466 Doi 10.1038/s41598-019-47607-5

56 Narasimhan S, Guo JL, Changolkar L, Stieber A, McBride JD, Silva LV, He Z, Zhang B, Gathagan RJ, Trojanowski JQ, et al. (2017) Pathological Tau Strains from Human Brains Recapitulate the Diversity of Tauopathies in Nontransgenic Mouse Brain. J Neurosci 37: 11406-11423 Doi 10.1523/JNEUROSCI.1230-17.2017

57 Radford H, Moreno JA, Verity N, Halliday M, Mallucci GR (2015) PERK inhibition prevents tau-mediated neurodegeneration in a mouse model of frontotemporal dementia. Acta Neuropathol 130: 633-642 Doi 10.1007/s00401-015-1487-z

58 Rashid HO, Yadav RK, Kim HR, Chae HJ (2015) ER stress: Autophagy induction, inhibition and selection. Autophagy 11: 1956-1977 Doi 10.1080/15548627.2015.1091141

59 Rauch JN, Luna G, Guzman E, Audouard M, Challis C, Sibih YE, Leshuk C, Hernandez I, Wegmann S, Hyman BT, et al. (2020) LRP1 is a master regulator of tau uptake and spread. Nature 580: 381-385 Doi 10.1038/s41586-020-2156-5

60 Riggs AC, Bernal-Mizrachi E, Ohsugi M, Wasson J, Fatrai S, Welling C, Murray J, Schmidt RE, Herrera PL, Permutt MA (2005) Mice conditionally lacking the Wolfram gene in pancreatic islet beta cells exhibit diabetes as a result of enhanced endoplasmic reticulum stress and apoptosis. Diabetologia 48: 2313-2321 Doi 10.1007/s00125-005-1947-4

61 Sakakibara Y, Sekiya M, Fujisaki N, Quan X, Iijima KM (2018) Knockdown of wfs1, a fly homolog of Wolfram syndrome 1, in the nervous system increases susceptibility to age- and stress-induced neuronal dysfunction and degeneration in Drosophila. PLoS Genet 14: e1007196 Doi 10.1371/journal.pgen.1007196

62 Sanders DW, Kaufman SK, DeVos SL, Sharma AM, Mirbaha H, Li A, Barker SJ, Foley AC, Thorpe JR, Serpell LC, et al. (2014) Distinct tau prion strains propagate in cells and mice and define different tauopathies. Neuron 82: 1271-1288 Doi 10.1016/j.neuron.2014.04.047

63 Sardiello M, Palmieri M, di Ronza A, Medina DL, Valenza M, Gennarino VA, Di Malta C, Donaudy F, Embrione V, Polishchuk RS, et al. (2009) A gene network regulating lysosomal biogenesis and function. Science 325: 473-477 Doi 10.1126/science.1174447

64 Scrivo A, Bourdenx M, Pampliega O, Cuervo AM (2018) Selective autophagy as a potential therapeutic target for neurodegenerative disorders. Lancet Neurol 17: 802-815 Doi 10.1016/S1474-4422(18)30238-2

65 Settembre C, Di Malta C, Polito VA, Garcia Arencibia M, Vetrini F, Erdin S, Erdin SU, Huynh T, Medina D, Colella P, et al. (2011) TFEB links autophagy to lysosomal biogenesis. Science 332: 1429-1433 Doi 10.1126/science.1204592

66 Stancu IC, Vasconcelos B, Terwel D, Dewachter I (2014) Models of beta-amyloid induced Tau-pathology: the long and "folded" road to understand the mechanism. Mol Neurodegener 9: 51 Doi 10.1186/1750-1326-9-51

67 Stranahan AM, Mattson MP (2010) Selective vulnerability of neurons in layer II of the entorhinal cortex during aging and Alzheimer's disease. Neural Plast 2010: 108190 Doi 10.1155/2010/108190

68 Takeda K, Inoue H, Tanizawa Y, Matsuzaki Y, Oba J, Watanabe Y, Shinoda K, Oka Y (2001) WFS1 (Wolfram syndrome 1) gene product: predominant subcellular localization to endoplasmic reticulum in cultured cells and neuronal expression in rat brain. Hum Mol Genet 10: 477-484 Doi 10.1093/hmg/10.5.477

69 Terasmaa A, Soomets U, Oflijan J, Punapart M, Hansen M, Matto V, Ehrlich K, Must A, Koks S, Vasar E (2011) Wfs1 mutation makes mice sensitive to insulin-like effect of acute valproic acid and resistant to streptozocin. J Physiol Biochem 67: 381-390 Doi 10.1007/s13105-011-0088-0

70 Urano F (2016) Wolfram Syndrome: Diagnosis, Management, and Treatment. Curr Diab Rep 16: 6 Doi 10.1007/s11892-015-0702-6

71 Vonsattel JP, Del Amaya MP, Keller CE (2008) Twenty-first century brain banking. Processing brains for research: the Columbia University methods. Acta Neuropathol 115: 509-532 Doi 10.1007/s00401-007-0311-9

72 Xu Y, Du S, Marsh JA, Horie K, Sato C, Ballabio A, Karch CM, Holtzman DM, Zheng H (2020) TFEB regulates lysosomal exocytosis of tau and its loss of function exacerbates tau pathology and spreading. Mol Psychiatry: Doi 10.1038/s41380-020-0738-0

73 Yamada T, Ishihara H, Tamura A, Takahashi R, Yamaguchi S, Takei D, Tokita A, Satake C, Tashiro F, Katagiri H, et al. (2006) WFS1-deficiency increases endoplasmic reticulum stress, impairs cell cycle progression and triggers the apoptotic pathway specifically in pancreatic beta-cells. Hum Mol Genet 15: 1600-1609 Doi 10.1093/hmg/ddl081

74 Yamamoto A, Simonsen A (2011) The elimination of accumulated and aggregated proteins: a role for aggrephagy in neurodegeneration. Neurobiol Dis 43: 17-28 Doi 10.1016/j.nbd.2010.08.015

75 Yang DS, Lee JH, Nixon RA (2009) Monitoring autophagy in Alzheimer's disease and related neurodegenerative diseases. Methods Enzymol 453: 111-144 Doi 10.1016/S0076-6879(08)04006-8

76 Yoshiyama Y, Higuchi M, Zhang B, Huang SM, Iwata N, Saido TC, Maeda J, Suhara T, Trojanowski JQ, Lee VM (2007) Synapse loss and microglial activation precede tangles in a P301S tauopathy mouse model. Neuron 53: 337-351 Doi 10.1016/j.neuron.2007.01.010

77 Yu G, Wang LG, Han Y, He QY (2012) clusterProfiler: an R package for comparing biological themes among gene clusters. OMICS 16: 284-287 Doi 10.1089/omi.2011.0118

Figure 1

Click here to access/download;figure;Figure 1.tif

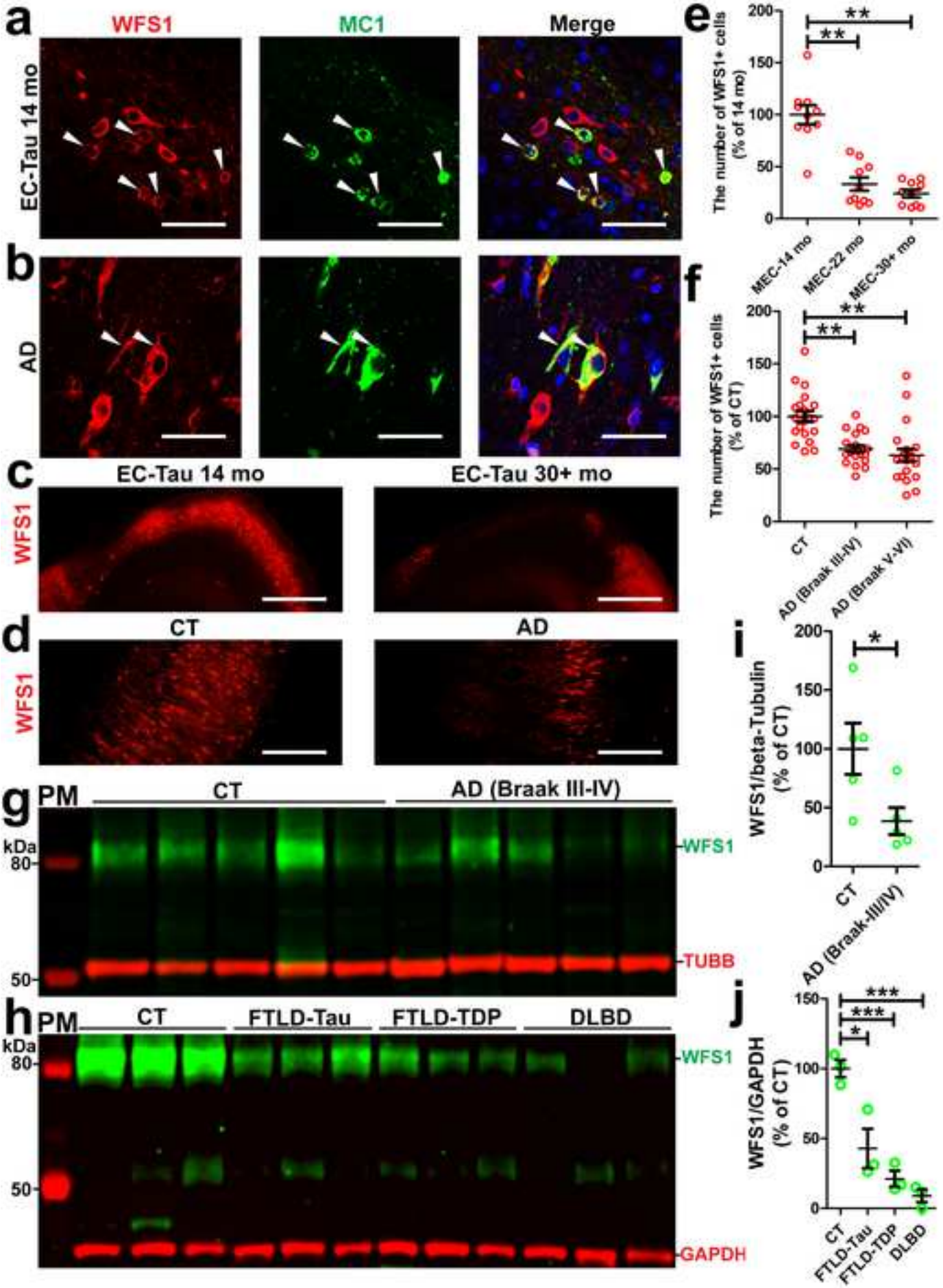

Figure 2

Click here to access/download;figure;Figure 2.tif

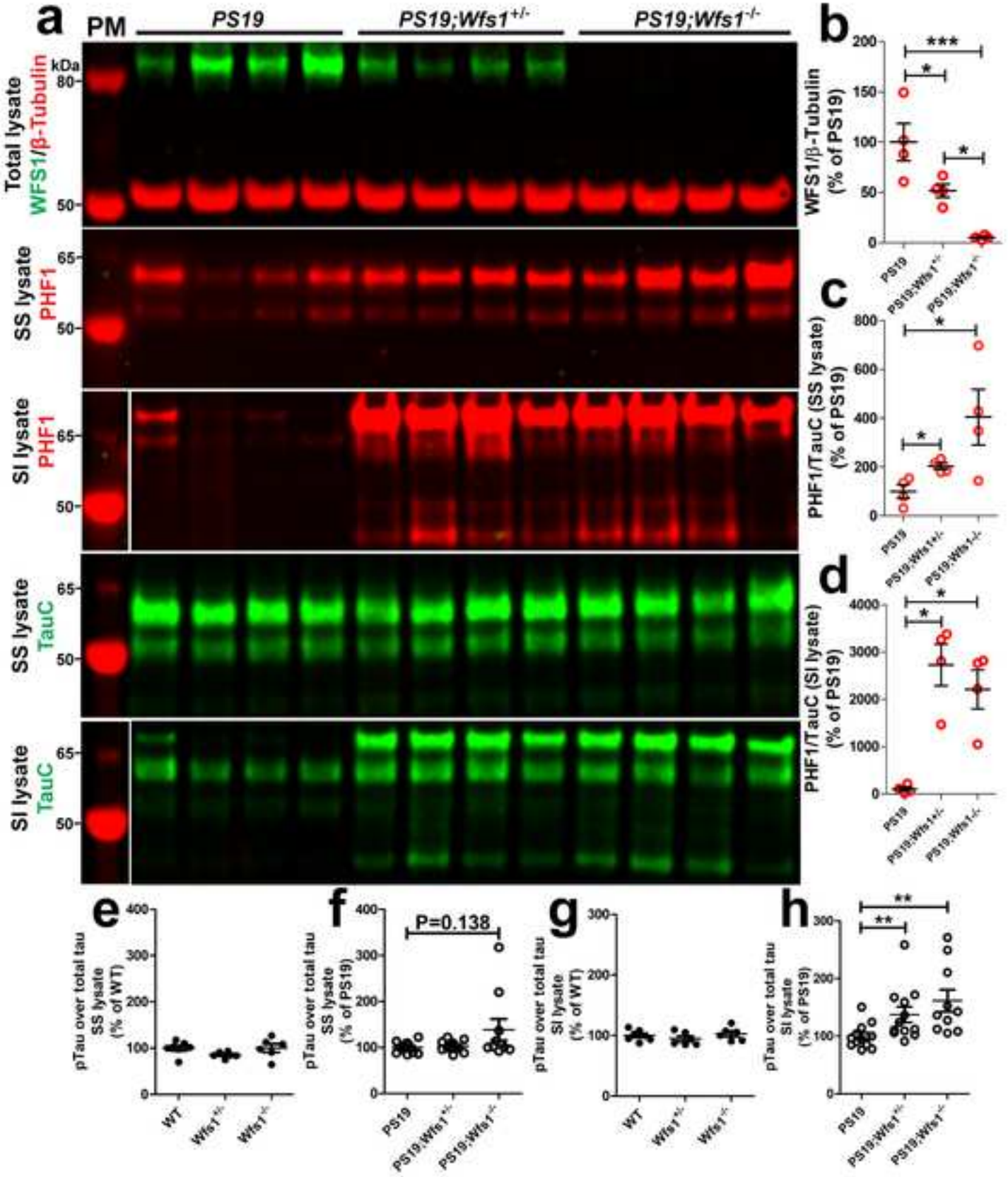

Figure 3

Click here to access/download;figure;Figure 3.tif

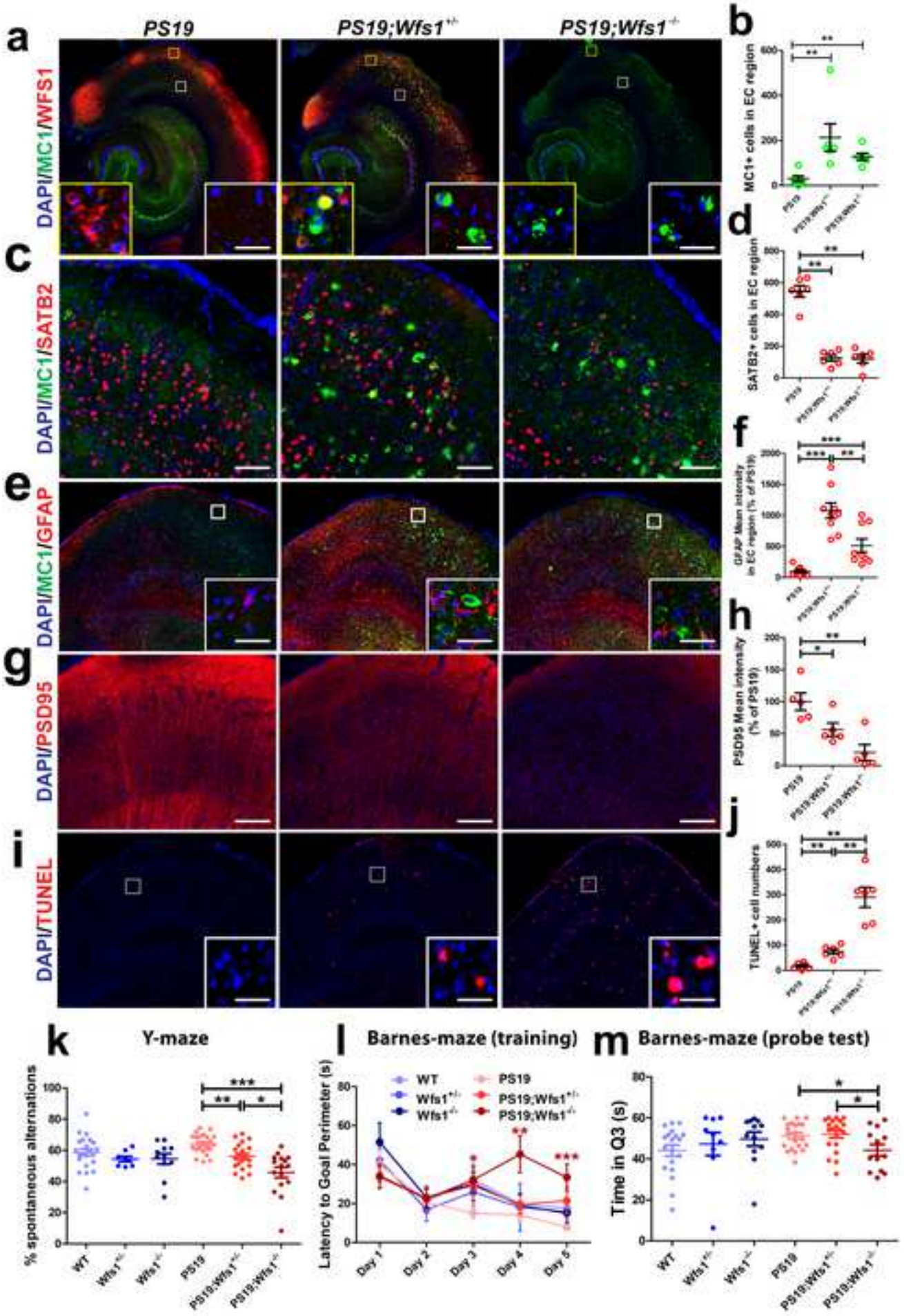

Figure 4

Click here to access/download;figure;Figure 4.tif

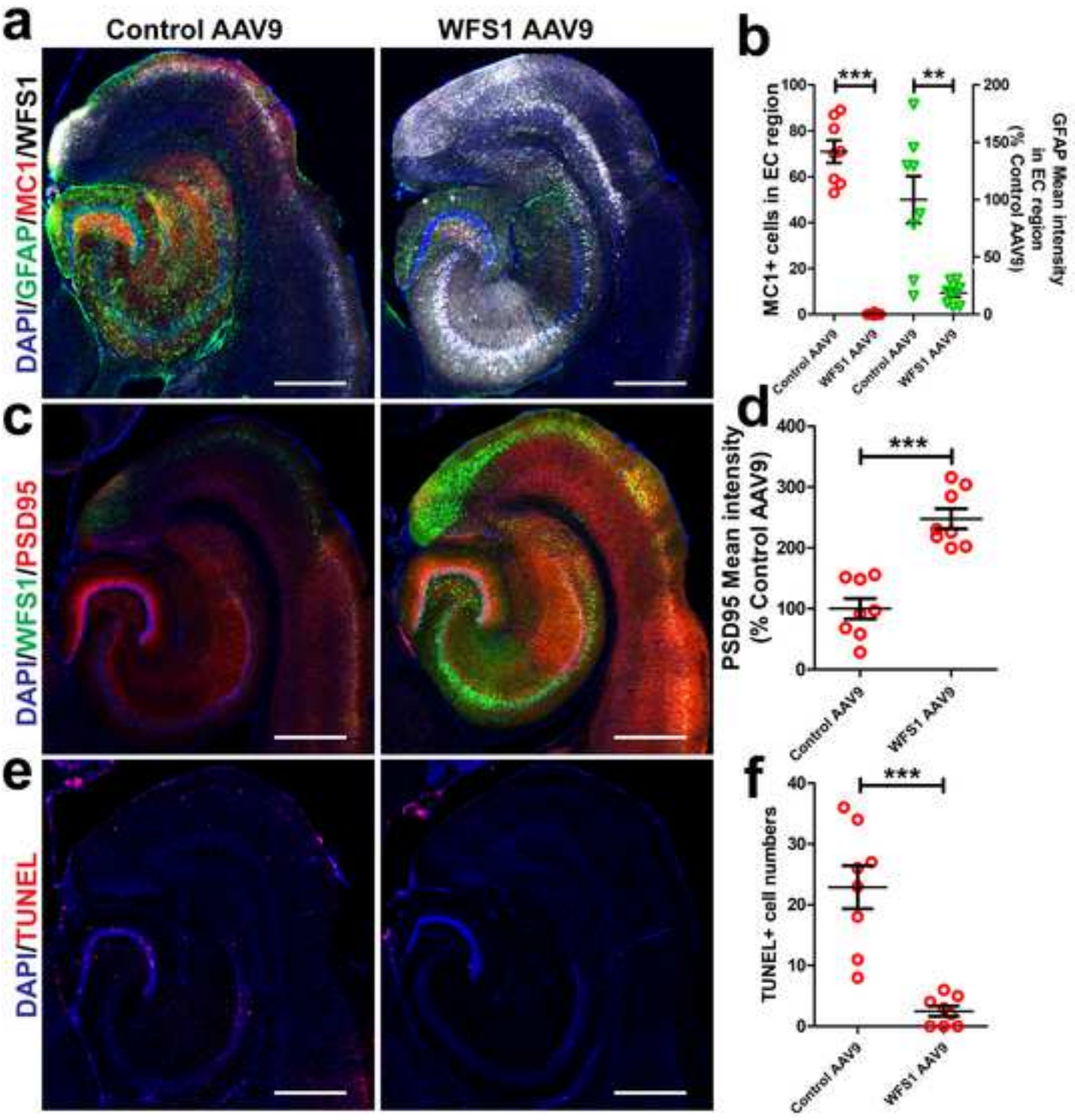

Figure 5

Click here to access/download;figure;Figure 5.tif

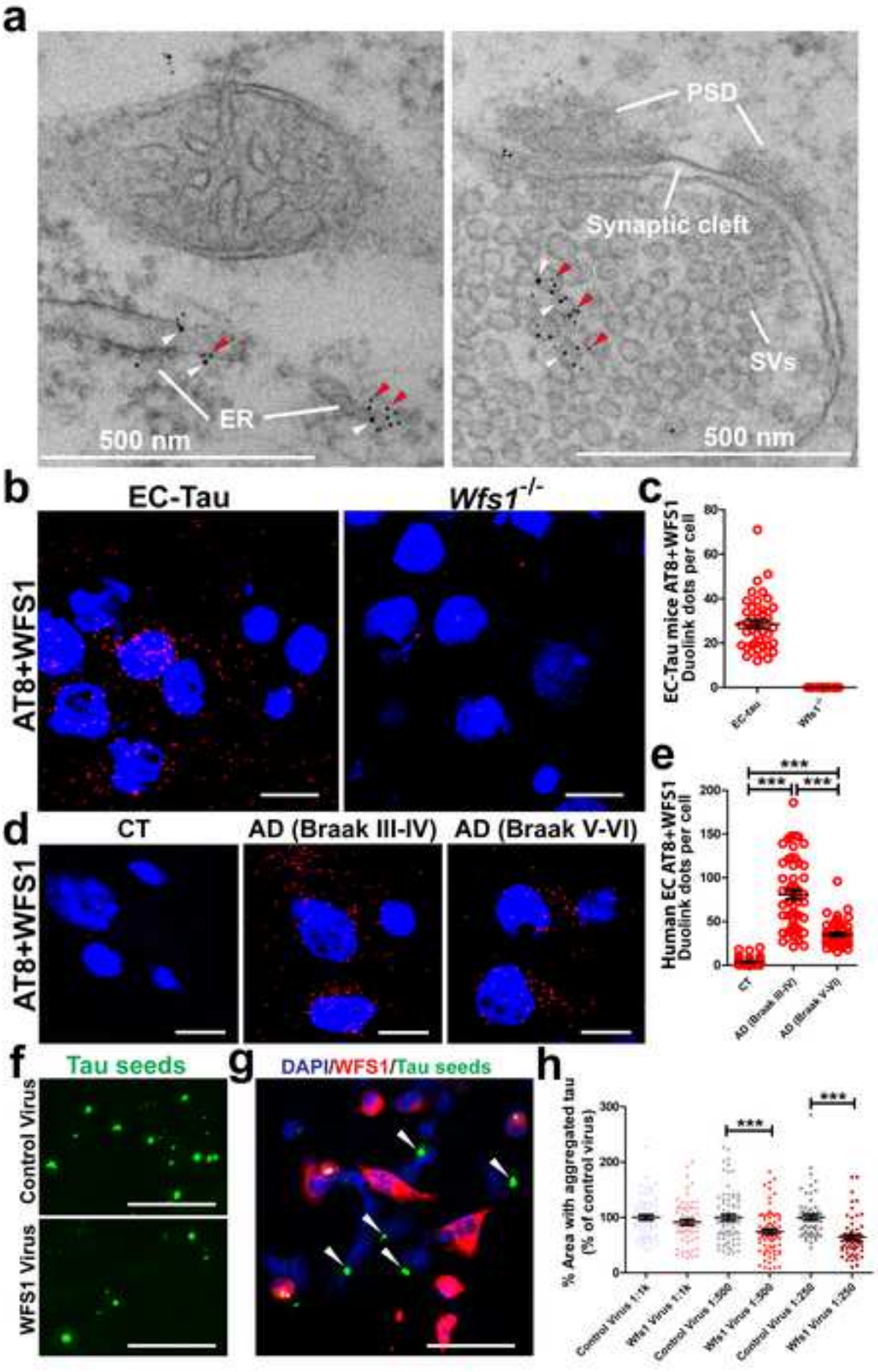

Figure 6

Click here to access/download;figure;Figure 6.tif

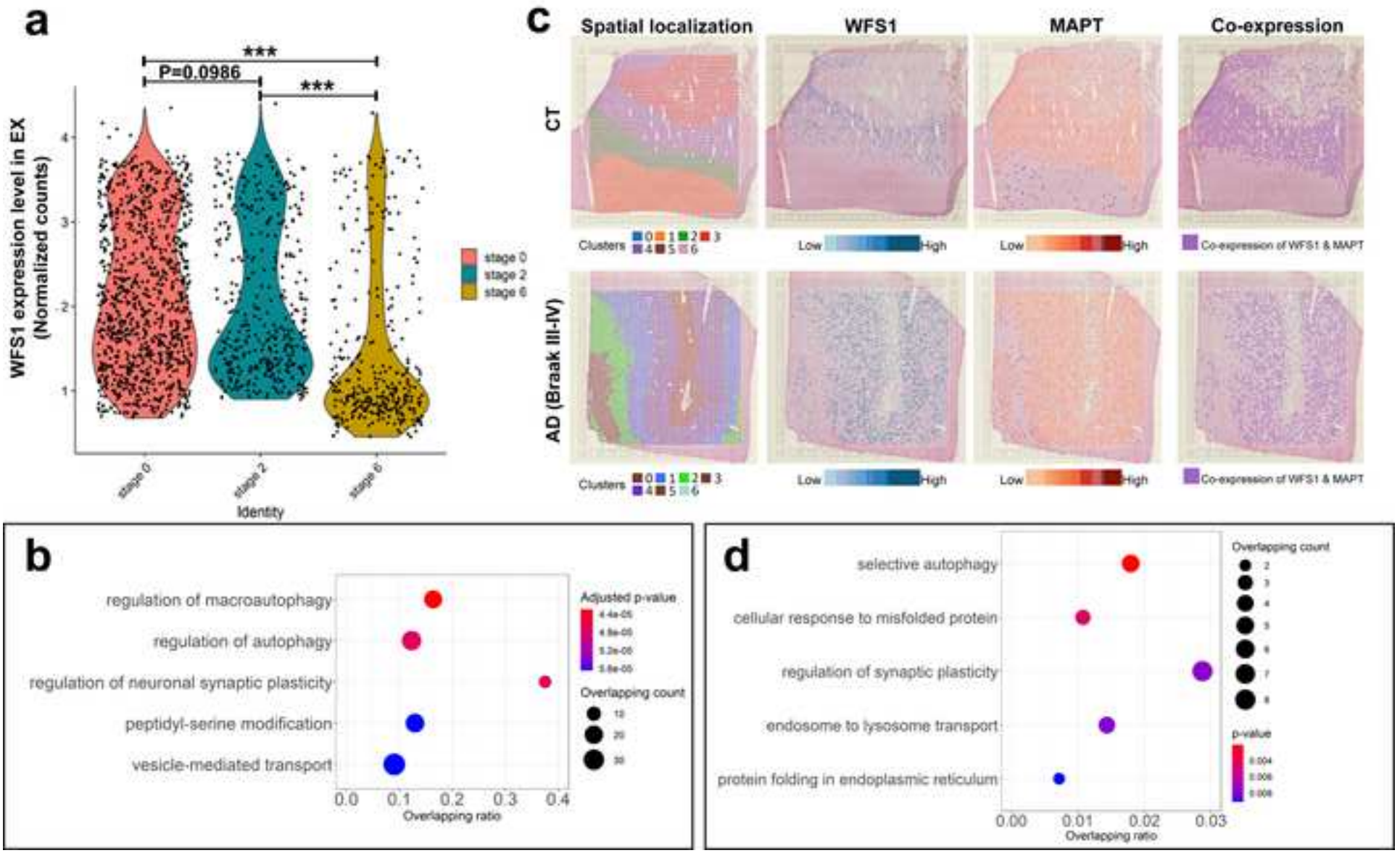

Figure 7

Click here to access/download;figure;Figure 7.tif

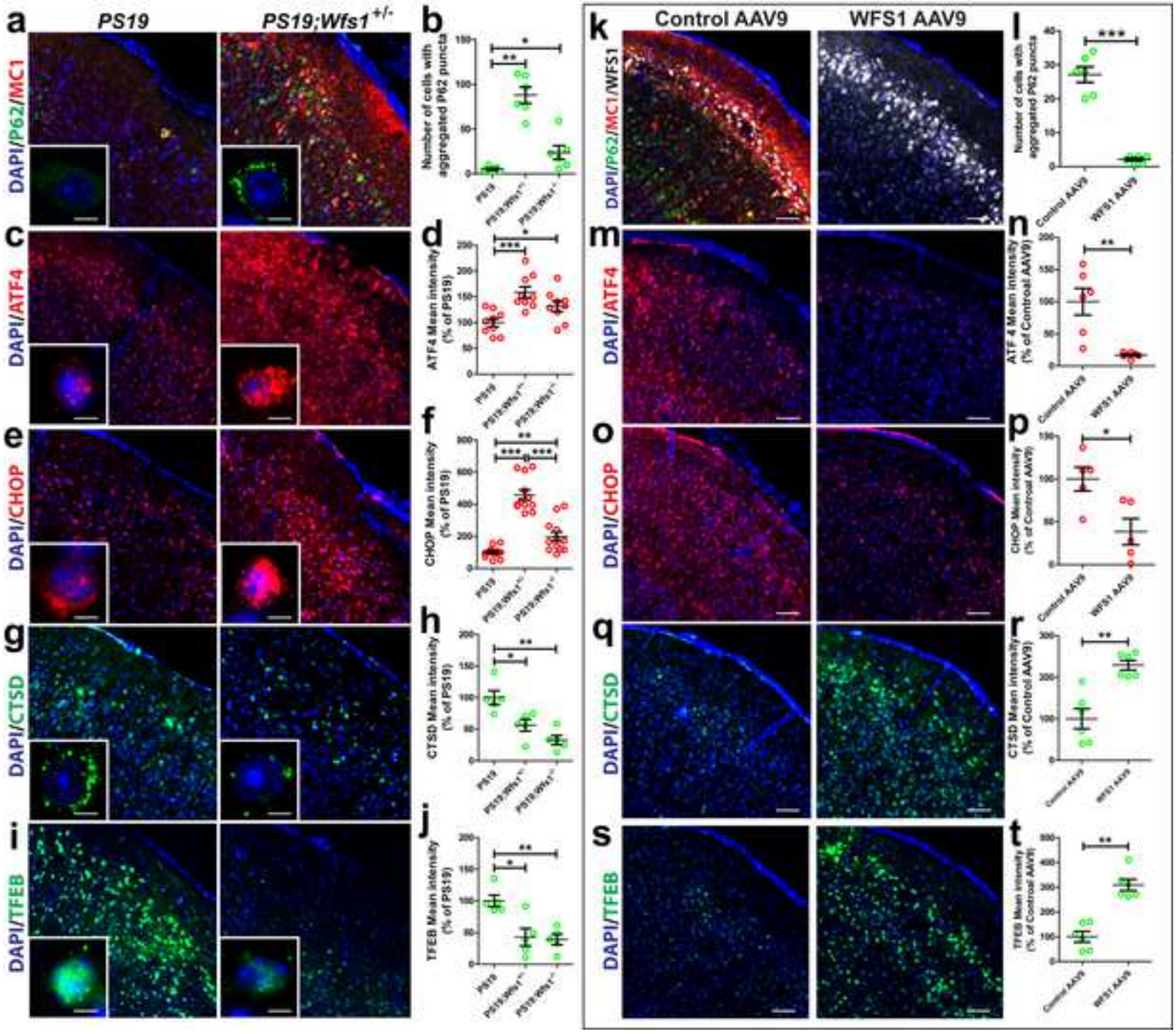

Figure 8

Click here to access/download;figure;Figure 8.tif

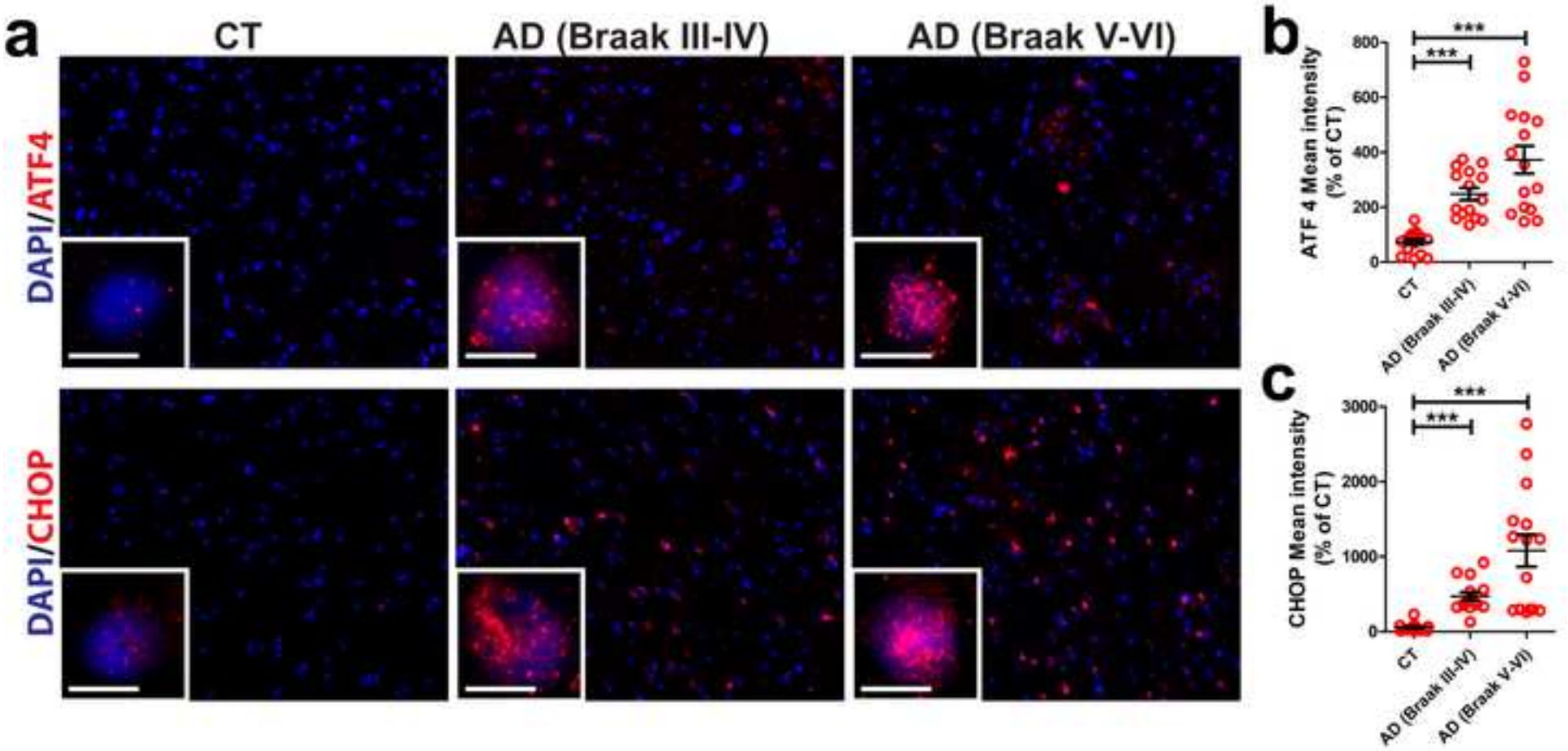

attachment to manuscript

Click here to view linked References